

TOPICAL REVIEW

## Brief overview of electrochemical potential in lithium ion batteries

To cite this article: Jian Gao *et al* 2016 *Chinese Phys. B* **25** 018210

View the [article online](#) for updates and enhancements.

### Related content

- [Lithium-ion transport in inorganic solid state electrolyte](#)  
Jian Gao, Yu-Sheng Zhao, Si-Qi Shi *et al.*
- [Current computational trends in polyanionic cathode materials for Li and Na batteries](#)  
Sudip Chakraborty, Amitava Banerjee, Teeraphat Watcharatharapong *et al.*
- [Multi-scale computation methods: Their applications in lithium-ion battery research and development](#)  
Siqi Shi, Jian Gao, Yue Liu *et al.*

### Recent citations

- [Promoting the electrochemical performance of LiNi<sub>0.8</sub>Co<sub>0.1</sub>Mn<sub>0.1</sub>O<sub>2</sub> cathode via LaAlO<sub>3</sub> coating](#)  
Yong-Chun Li *et al*
- [Advances in Structure and Property Optimizations of Battery Electrode Materials](#)  
Jia Shen Meng *et al*
- [Lithium battery chemistries enabled by solid-state electrolytes](#)  
Arumugam Manthiram *et al*

# Brief overview of electrochemical potential in lithium ion batteries\*

Jian Gao(高健)<sup>1,2</sup>, Si-Qi Shi(施思齐)<sup>3,2</sup>, and Hong Li(李泓)<sup>1,†</sup>

<sup>1</sup>*Institute of Physics, Chinese Academy of Sciences, Beijing 100190, China*

<sup>2</sup>*Materials Genome Institute, Shanghai University, Shanghai 200444, China*

<sup>3</sup>*School of Materials Science and Engineering, Shanghai University, Shanghai 200444, China*

(Received 15 May 2015; revised manuscript received 20 July 2015; published online 7 December 2015)

The physical fundamentals and influences upon electrode materials' open-circuit voltage (OCV) and the spatial distribution of electrochemical potential in the full cell are briefly reviewed. We hope to illustrate that a better understanding of these scientific problems can help to develop and design high voltage cathodes and interfaces with low Ohmic drop. OCV is one of the main indices to evaluate the performance of lithium ion batteries (LIBs), and the enhancement of OCV shows promise as a way to increase the energy density. Besides, the severe potential drop at the interfaces indicates high resistance there, which is one of the key factors limiting power density.

**Keywords:** lithium ion batteries, open circuit voltage, Fermi energy level, electrochemical potential

**PACS:** 82.47.Aa, 05.70.-a

**DOI:** [10.1088/1674-1056/25/1/018210](https://doi.org/10.1088/1674-1056/25/1/018210)

## 1. Introduction

Lithium ion batteries (LIBs) celebrated their twenty-fifth birthday this year, and among the most promising electrochemical cells which are expected to replace the traditional fossil fuels in transportation, as well as energy storage for intermittent renewable energy such as solar or wind power, to satisfy urgent environmental demands. In addition, they have been widely applied in portable consumer electronic products. Although LIBs have achieved the dominant position in cell markets as compared with lead-acid and Ni-MH cells, they are still restrained by insufficient energy density and power density, and are in urgent need of further guarantees of safety. This review will concentrate on how the above problems can be considered and dealt with from the aspect of electrochemical potential.

The first requirement, energy density, can be realized by developing novel electrode materials. Anodes (modified carbons are widely adopted) generally have higher capacities than common cathodes. The next-generation anode materials, lithium metal or silicon-(active metal) alloys, even represent better hope for quite great enhancement in capacity. As a result, the bottleneck of energy density always lies in the commercial cathodes such as  $\text{LiCoO}_2$ ,  $\text{LiFePO}_4$  and  $\text{LiMn}_2\text{O}_4$ . Given the equation  $E = Vq$ , where  $E$  is energy,  $V$  is voltage, and  $q$  is the electronic charge quantity, there are two methods to improve the energy density, of which one is to enrich the Li content (Li-rich cathodes), and the other is to increase the output voltage (high-voltage cathodes). The latter is focused on for its relationship to the electrochemical potential problems.

With the given composition and structure, the output voltage of a compound can be theoretically identified, making it possible to design cathode materials through calculations. Then the maintenance of framework structure to assure the reversibility is the only problem left to be taken into consideration for the practical cathodes, which can be investigated by the lithium (de)intercalation phase diagram, influenced by both thermodynamic and kinetic factors. However, the output voltage, which is determined by anode and cathode, also needs to be within the electrochemical windows of electrolyte to suppress the decomposition and side reaction at the interfaces. As a result, new developments in electrolytes and electrolytic additives are also in urgent demand to realize compatibility with the novel cathodes.

The second requirement, power density, is not related so directly to the electrochemical potential. However, the high-rate charge and discharge usually bring about side reactions and subsequent aging and capacity-fade at the interfaces, which can be attributed to kinetic stability problems influenced by the sharp potential drop across the interphases, where a high proportion of a full cell system's resistance lies. In addition, the potential variation at the interface modulates the lithium diffusion mechanism there.

The safety issue, which is regarded as the third requirement, promises to be solved by the replacement of electrolytic solutions by solid-state electrolytes. However, the high solid-solid interface resistance is often the predominant limitation of actual LIBs' performance. By now, the space charge layer of solid-solid interphases, which comprises the complicated

\*Project supported by the National Natural Science Foundation of China (Grant Nos. 51325206 and 51372228), National Basic Research Program of China (Grant No. 2012CB932900), Shanghai Pujiang Program, China (Grant No. 14PJ1403900).

†Corresponding author. E-mail: [hli@aphy.iphy.ac.cn](mailto:hli@aphy.iphy.ac.cn)

© 2016 Chinese Physical Society and IOP Publishing Ltd

<http://iopscience.iop.org/cpb> <http://cpb.iphy.ac.cn>

problems such as chemical potential, electric potential as well as electrochemical potential, still remains unclear. Further understanding of solid–solid space charge layer and the electrochemical potential variation therein can contribute to the application of solid-state electrolytes and thus improve safety.

The problems related to electrochemical potential in LIBs are reviewed, including the output voltage of electrodes, the spatial distribution of electrochemical potential in the full cell and its possible effects on the performance. The relevant factors affecting the output voltage are presented. Then applications such as high-voltage cathodes, anodes and electrodes

based on conversion reactions are summarized. Moreover, the reasons for discrepancies between calculated results and experiments are discussed, involving thermodynamic and kinetic factors, as well as the single electron approximation of Kohn–Sham equation within the density functional theory (DFT) framework.

## 2. Hierarchical structure of lithium ion batteries

As shown in Fig. 1, the full cell of a lithium ion battery mainly contains: A-current collector, B-anode, C-electrolyte, D-cathode, and E-current collector.

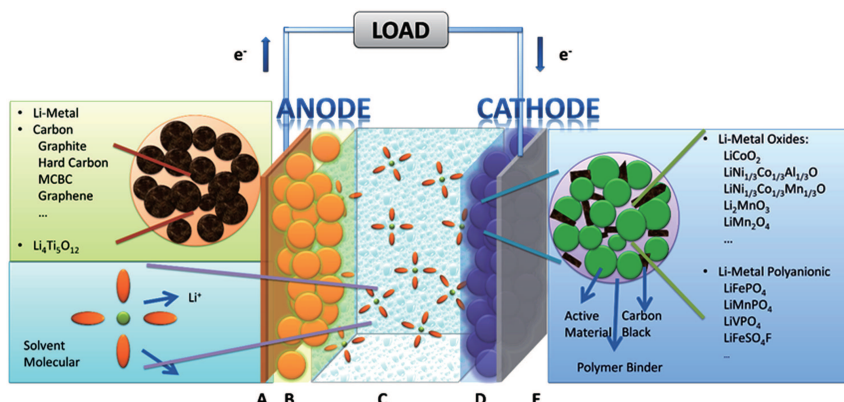


**Fig. 1.** The hierarchical structure of lithium ion batteries.

The most common sandwich structural cell contains cathode–electrolyte–anode. In the case of LIB with the organic electrolytic solution (including solvents and Li salts) as the electrolyte, the full sandwich cell is assembled by rolling, folding or stacking and placed within a hermetically sealed casing. Then the porous material lies naturally across the whole cell to guarantee the wettability of solid matrix of both electrodes and separator filled with electrolytic solution. Outside the porous sandwich is the current collector, usually Cu foil at the anode side and Al at the cathode side. The construction of each electrode begins with the active material powder of spherical or ellipsoid particles with diameters ranging from nanometers to micrometers. The powder is mixed with conductive additives and binders, and the completed mixture holds the liquid-filled pores throughout, referred to as “porous electrode”. For the porous electrode, the active material is at the core, which is chosen to drive the overall electrochemical reaction of the battery to produce the output electrical current, preserving structural stability during the  $\text{Li}^+$  intercalation/deintercalation. In the case of polymer cells, only the electrolyte is replaced by solid/gel polymer by contrast.

Inorganic all-solid-state batteries can also be fabricated into the sandwich structure, just similar to their counterparts with organic electrolytic solution, while the electrolytes of the former are made of inorganic ionic conductor ceramic pellets.

Because there is no electrolytic solution to wet the electrodes, the active materials should be mixed with solid electrolytes together with conductive additives and binders instead. The alternative strategy to realize the all-solid-state battery is to adopt the thin film structure, where the cathode and electrolyte are deposited onto current collectors in sequence, and Li metal or Li alloys can be adhered as anode. Film all-solid-state batteries have advantages such as simple construction of structure, freedom from the binders and conductive additives, and the service life of as much as ten thousand cycles.<sup>[1]</sup> Besides the sandwich-structure and thin film batteries, three dimensional (3D) integrated all-solid-state batteries exist as promising candidates with higher energy density, for the significantly increased surface area.<sup>[2]</sup> Figure 2 shows the different forms of inorganic all-solid-state batteries. Given that they always share the same fundamental problems concerning the electrochemical potential in LIBs, they will not be discussed individually in the following.

The principal operating mechanism of batteries is shown in Fig. 1: Li ions shuttle like a “rocking chair” between two electrodes. During the discharge, Li ions deintercalate from the anode and intercalate into the cathode, as the result of the  $\text{Li}^+$  chemical potential difference between the two electrodes, and this process decreases the energy of the full cell. With respect to maintaining electrical neutrality, electrons leave the

anode simultaneously and flow into the cathode through the external circuit, which provides electrical energy to the load. The general effect of discharge is to convert chemical energy into electrical energy by means of the redox reaction of electrodes driven by the chemical potential difference between cathodes and anodes. The opposite is true during the charge. Here we will focus on the electrochemistry-related problems such as charge transfer and mass transport process (both in bulk and at the interface) of the electrochemical system, the electrode's structural transformation and phase transition during the Li ion (de)intercalation, and the relationship between the electrical and chemical effects at the various time and space scales of the full cell.

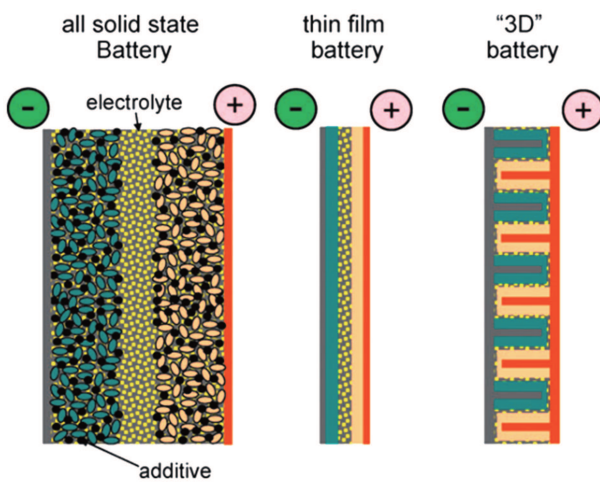


**Fig. 2.** A schematic representation of different battery configurations using solid electrolytes. Current collectors are depicted in grey (positive) and brown (negative), and active materials in pink and green, respectively.<sup>[3]</sup>

### 3. Open circuit voltage

Only under the equilibrium state condition can the system be thermodynamically reversible, thus one thermodynamic pa-

rameter should be introduced if the thermodynamic aspects of electrochemical systems are of interest. When batteries doing electric work outside, electrons are powered by the potential difference, and the directional aspect should be assigned to this parameter to describe the reaction other than the physical system. This parameter can be fixed as electromotive force (EMF).

The reversibility can be reached by applying an infinite load resistance, then the potential difference between the ends of the battery's cathode and anode is defined as open circuit voltage (OCV). The infinite load resistance assures finite current. Providing the zero current, the electrochemical system can be ensured of reversibility, then this potential difference is equal to EMF, with the positive or negative value indicating the actual reaction direction. OCV is an observable parameter used more commonly than EMF in LIB investigations. However, every process in practice occurs at finite rates with finite current (nonzero), so the internal resistance cannot be neglected. As a result, this so-called "OCV", which is usually misused in experiments by ignoring the sufficient load resistance, is not exact and actually lower in value than theoretical OCV, or to say, EMF. The OCV is bound up with SOC, and usually decreases accompanied by the discharge process.

Theoretically, given the basic assumption of electrical neutrality in the electrode particles, which is guaranteed by the small sizes of particles and dispersed connective conductive additives, we can calculate the OCV/EMF (in the following sections, only the term OCV is used habitually) from the perspectives of both Fermi energy level and Gibbs free energy respectively, arriving at the same conclusion, as shown in Fig. 3.

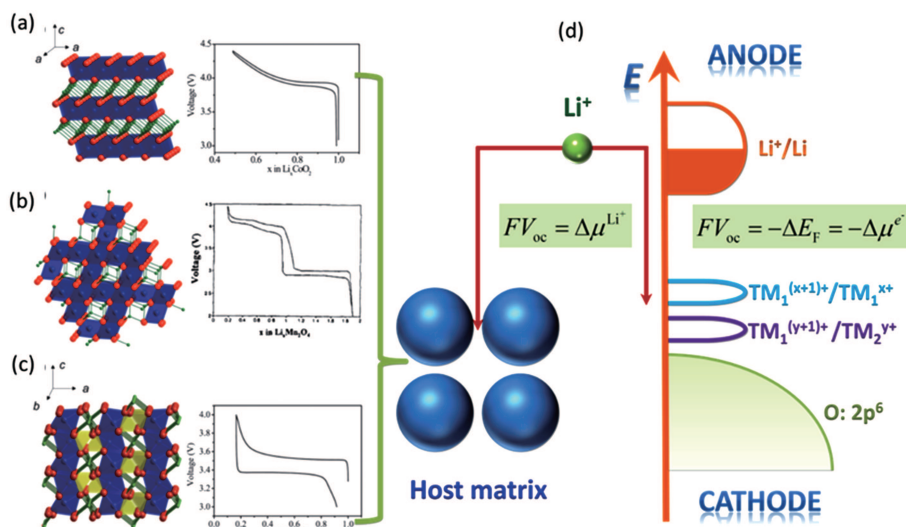


**Fig. 3.** Crystalline structures and voltage–composition curves of (a) layered-LiCoO<sub>2</sub>; (b) spinel-LiMn<sub>2</sub>O<sub>4</sub>; (c) olivine-LiFePO<sub>4</sub>.<sup>[4]</sup> (d) Open circuit voltage: from the aspect of Fermi energy level or electrochemical potential of Li (adapted from Ref. [5]).

### 3.1. Fermi energy level perspective

Fermi energy level refers to the energy when the electron occupation probability equals 0.5 in the electronic energy level (Fermi–Dirac distribution). As the distribution is similar to a step function, it can be approximately considered that electrons mainly fill the energy levels below Fermi energy level at the finite temperature, while levels above are unoccupied. Then the levels in the vicinity occupied by the probability ranging from 0 to 1 are called “transition state”. The lithium ion batteries referred to as “rocking chair” batteries, electrolytes play only the role of transporting lithium ions and are not involved in the electrochemical reaction. Ideally, during the discharge process, only the electrodes are taking part in the redox reaction, enabling electrons to flow through the external circuit in the direction from anodes with higher Fermi energy to cathode material with a lower one. Therefore, the open-circuit voltage of the cell system satisfies

$$FV_{oc} = -\Delta E_F = \mu_A^e - \mu_C^e, \quad (1)$$

where  $F$  represents Faraday’s constant. For the common solid electrode materials, the Fermi energy level depends on the material’s work function.

At the cathodes, the charge–discharge’s reversibility is realized by applying the transition metals to the Li-(de)intercalating materials, which enables itself to be stable within a wide range of Li concentration. The electronic configuration of the transition metal ion in cathode is  $3d4s$ , therefore the losing or gaining of electrons in  $d$ -electron manifold corresponds to the oxidation and reduction of transition metal. Electrons in  $3d$ -electron manifold display the localization character and have a narrow energy band due to the strong charge density Coulomb interaction. When the  $d$ -energy band is close to the  $p$ -energy band, covalent electrons mix with each other, which delocalizes electrons and broadens the band structure, causing the Fermi energy level to move into the conduction band. When electrons from an anode with higher Fermi energy level fill into a cathode with lower Fermi energy level, only the electrons near the Fermi energy level change state rather than filled or empty additional band. The electrons’ transfer at only the Fermi energy level will not lead to an obvious changing in the OCV voltage profile as the SOC evolves. In fact, the obvious change of voltage profile to the “S” type is based on alteration of the configuration of the crystal lattice, accompanied by a consequent shift of electronic structure. For materials with electron localization, the Fermi energy level lies between the valence and conduction bands. Taking the discharge process of the battery with Li anode and LiFePO<sub>4</sub> cathode as an example, while electrons are flowing out of the anode to fill the cathode, they occupy the additional empty band (Fe<sup>3+</sup>) which was originally the valence band, because the conduction band is filled in Fe<sup>2+</sup>. From the perspective of real space, electrons are localized to the single Fe<sup>3+</sup>,

contributing to the formation of Fe<sup>2+</sup>, and attracting the neighboring unstable Li<sup>+</sup> to form LiFePO<sub>4</sub>. Note that the electrons hop in (Li)FePO<sub>4</sub> as “small polarons”, arising from the fine tuning of the surrounding crystal lattices. The propulsion of phase interface is driven by the stress field, which brings out the so-called two-phase reaction, exhibiting an “L” type voltage profile and a stable OCV during this discharge process. Since LiFePO<sub>4</sub> and FePO<sub>4</sub> hold a certain degree of reduced miscibility gaps arising from the dynamics factors, a limited solid solution occurs, and thus appears the delocalization of electrons to some extent. As shown in experimental results, both side knees of the “L” type voltage profile will end up with a limited range of “S” type curve. Next the physics meanings of different types of voltage profiles is demonstrated in detail from the aspect of Gibbs free energy.

At the anodes, the various analysis methods should be taken to match the specific reaction mechanisms during the charge/discharge process, such as alloying reaction (e.g., Li, C, Si, and so on, summarized in Ref. [6]), (de)lithiation reaction (Li<sub>4</sub>Ti<sub>5</sub>O<sub>12</sub>),<sup>[7]</sup> conversion reaction (defined as that there exists at least two products).<sup>[8,9]</sup> (i) Li anode: The Li metal anode contains a large number of itinerant electrons near the Fermi surface, and will not experience a phase transition during the charge/discharge process; thus the Fermi energy level keeps unchanged unless considering the morphology factors. (ii) Li binary alloy anode: The binary system usually experiences a series of phase transitions when Li is in the alloy, indicating the discontinuous changes of Fermi energy level. The phase diagrams and voltage profiles of Li–C and Li–Si are illustrated in Refs. [10]–[12] respectively as examples. The most common carbon-based graphite anode with high electrical conductivity keeps structural stability during staged phase transition cycles. However, the silicon-based anode usually endures the high volume expansion, resulting in great changes in morphology and the totally different actual voltage profile from the theoretical data.<sup>[12]</sup> (iii) The (de)lithiation-based anode: Its reaction mechanism is quite similar to that of cathodes mentioned above, and Li<sub>4</sub>Ti<sub>5</sub>O<sub>12</sub> will be illustrated from aspect of Gibbs free energy in the next section. (iv) Conversion reaction-based anode: In addition to complicated multi-electron transfer, great changes of morphology contribute to the modulation of voltage profile, called the kinetic hysteresis effect.

### 3.2. Gibbs free energy perspective

To maintain the electrical neutrality, the injections and ejections of electrons and ions from electrodes must appear simultaneously, with the differences of Fermi energy levels and chemical potentials respectively as the driving forces, and the latter can be deduced from relative Gibbs free energies of reactants and products. So the relationship between Fermi energy level and Gibbs free energy is as follows: At the isothermal-isobaric process in the cells, the maximum electrical work gen-

erated by the electrode reaction is equal to non-volume work generated by the change of the reaction system, namely the change of molar free energy ( $\Delta_f G$ ).

The theoretical electric potential is defined by OCV as  $V_{OC}$ , and the work done by the cell system to surrounding environment is  $nFV_{OC}$ ; thus the change of the Gibbs free energy can be defined as the negative value of the output work in thermodynamics, therefore,

$$\Delta G = -nFV_{OC}. \quad (2)$$

In LIBs, supposing that the chemical formula of the cathode can be written as  $\text{Li}_x\text{TM}_y\text{X}_z$ , for an arbitrary SOC, the open-circuit voltage can be defined as

$$\begin{aligned} FV_{OC}(x) &= -[\mu_C^{\text{Li}}(x) - \mu_A^{\text{Li}}] \\ &= -\int_{x_1}^{x_2} [\mu_{\text{IC}}^{\text{Li}}(x) - \mu_A^{\text{Li}}] dx_{\text{Li}}|_{x_2 \rightarrow x_1=x}/(x_2 - x_1) \\ &= -[G_{\text{Li}_{x_2}\text{TM}_y\text{X}_z} - G_{\text{Li}_{x_1}\text{TM}_y\text{X}_z} \\ &\quad - (x_2 - x_1) G_{\text{Li}}]|_{x_2 \rightarrow x_1=x}/(x_2 - x_1) \\ &\equiv -\partial G(x)/\partial x. \end{aligned} \quad (3)$$

In fact, not all theoretical Gibbs free energy can be obtained easily for an arbitrary value  $x$ , due to the still unresolved problems of the Li-ion-occupied lattice sites and the resulting ordering structure at the given SOC, providing that different configurations will give rise to discrepancies in Gibbs free energy. As for the two-phase reaction, the respective Gibbs free energies can be easily obtained from the corresponding two phase structures, while for the solid solution reaction, only the average OCV can be estimated from initial and end configurations, without the details about instantaneous OCV for arbitrary configurations during the continuous intercalating/deintercalating of Li ions.

In order to quantitatively study the dependence of Gibbs free energy and the resulting Li chemical potential on the  $\text{Li}^+$  concentration, we first suppose a simple mechanical mixture of two pure components, where the Gibbs free energy of the mixture reads  $G^M = X_A G_A + X_B G_B$ . According to Gibbs' phase rule, in a system where two phases coexist, with fixed temperature and pressure, the system has no degrees of freedom, which leads to a constant chemical potential and the linear Gibbs free energy  $G^M$ , as shown by the green line in Figs. 4(a)–4(d). Secondly, considering the random mixing, configurational entropy  $\Delta S_m$  (shown by the pink line) should be included in total Gibbs free energy, as shown in Fig. 4(a), the term of  $-T\Delta S_m$  leads the simple two-phase mechanical mixture to the ideal solution. Next, when the effect of excess enthalpies  $\Delta H$  (shown by turquoise line in Figs. 4(b) and 4(c)) included, the total Gibbs free energy becomes  $G = G_M + \Delta H - T\Delta S_m$ . On one hand, when the excess enthalpy is negative, it will further reduce the free energy of the mixture in addition to  $-T\Delta S_m$  and the system results

in solid solution, as shown in Fig. 4(b). On the other hand, when the excess enthalpy is positive as shown in Fig. 4(c), the free energy has two minimum values at the composition of  $\alpha$  and  $\beta$ . At the composition between  $\alpha$  and  $\beta$ , the free energy of mechanical mixture  $\alpha + \beta$  is lower than the solid solution (Note that within that range the chemical potentials for each component are all the same). Namely, the phase separation occurs. However, at the two ends of the composition, a limited range of solution appears as the result of configuration entropy. When the lattice mismatch between A and B is too much, the positive excess enthalpy can be quite large, leading to a sharp enhancement of Gibbs free energy as shown in Fig. 4(d). Finally, strain and stress are usually important factors in consideration. Reducing the particle size to nanoscale can increase the structural tolerance of strain and stress, and thus restrain the phase separation.<sup>[13]</sup>

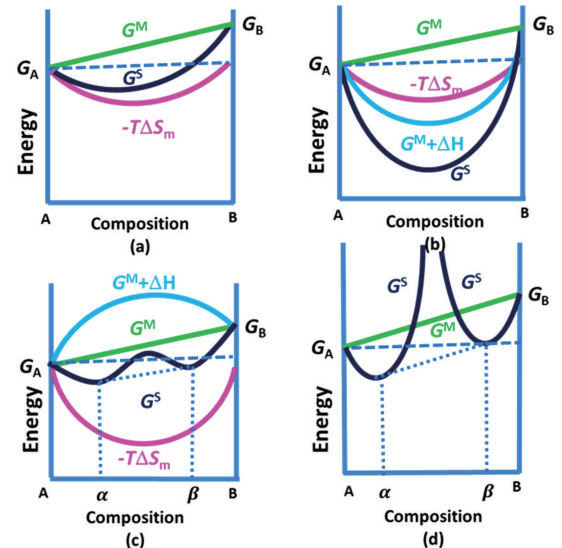


**Fig. 4.** Free-energy-composition diagrams for (a) ideal solution, (b) and (c) regular solutions, and (d) incomplete solid solution.

When the solid solution reaction occurs in the electrodes, it will exhibit a smoothly sloping voltage curve as shown in Fig. 5(b), the single phase system observes the Gibbs phase rule as: the number of degrees of freedom is 1 for the fixed temperature and pressure. From Eq. (3), the variation of the chemical potential with the  $\text{Li}^+$  concentration satisfies

$$V_{OC}(x) \equiv \frac{1}{F} \left( \frac{T\partial S(x)}{\partial x} - \frac{\partial H(x)}{\partial x} \right). \quad (4)$$

When, however, Li insertion is accompanied by a first-order phase transformation from a Li-poor phase  $\alpha$  to a Li-rich phase  $\beta$ , there are two local minima (assuming the host maintains the same crystal structure), as shown in Fig. 5(c). In the phase separation region (the range between the two minima), the total Gibbs free energy is the mechanical mixture of the two minima. As a result, a linear tangent with the constant partial derivative of  $\partial G(x)/\partial x$  leads to a plateau voltage profile as shown in Fig. 5(d),<sup>[14]</sup> which is consistent with

the equivalent chemical potentials of two phases in equilibrium. For this case of first-order transition, the nano-size effects have a significant influence on the voltage profile, and the miscibility gap is reduced because of the additional Gibbs free energy,<sup>[13,15,16]</sup> which may be caused by strain,<sup>[17]</sup> surface or interface energy,<sup>[18]</sup> or Li<sup>+</sup> concentration gradient in the diffuse interface,<sup>[19]</sup> as shown in Fig. 6.<sup>[7]</sup> The insertion chemical potentials are different along various crystal orientations near the surface, responsible for the more curved voltage profiles, as shown in Fig. 6(c).<sup>[7]</sup> In addition, the term of surface energy together with the distribution of particle sizes

will lead to a combined effect similar to that resulting from the solid solution,<sup>[20]</sup> and make a further step to account for the differences among the curved shapes as shown in Fig. 7,<sup>[7]</sup> especially for the cases that the phase transition occurs in separate individual small particles rather than evolving two-phases interfaces.<sup>[21]</sup> Under this condition, the phase transition appears continuously particle-by-particle, and the Gibbs free energy variation of each particle is influenced by the configuration entropy. The two factors together have a combined effect of hysteresis presented in the voltage profiles, also as shown in Fig. 7.<sup>[22]</sup>

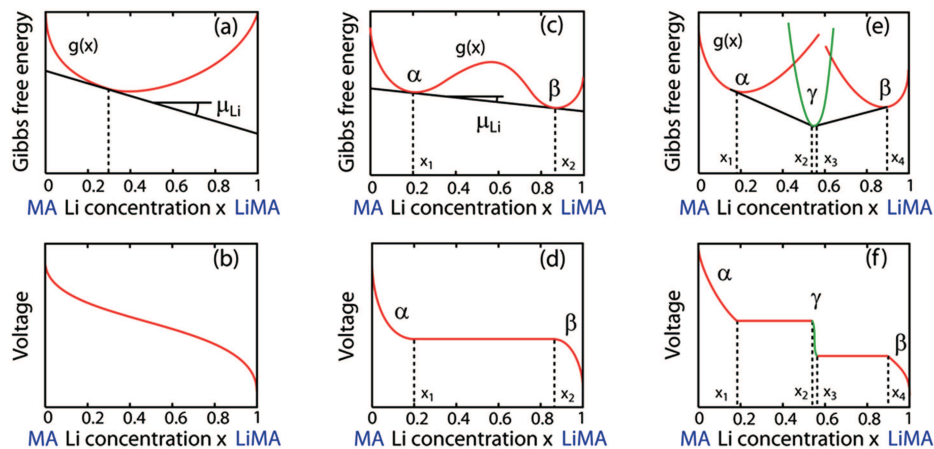


**Fig. 5.** Voltage curves are linearly related to the slope of the free energy of the electrode material. If the electrode host material forms a solid solution with Li as panel (a), it will exhibit a smooth sloping voltage curve as illustrated in panel (b). If, however, Li insertion is accompanied by a first-order phase transformation from a Li poor phase,  $\alpha$ , to Li rich phase,  $\beta$ , it will have a free energy curve as illustrated in panel (c), and resulting in a plateau in the voltage curve as illustrated in panel (d). Steps in the voltage profile appear if an intermediate phase is stable as in panels (e) and (f).<sup>[14]</sup>

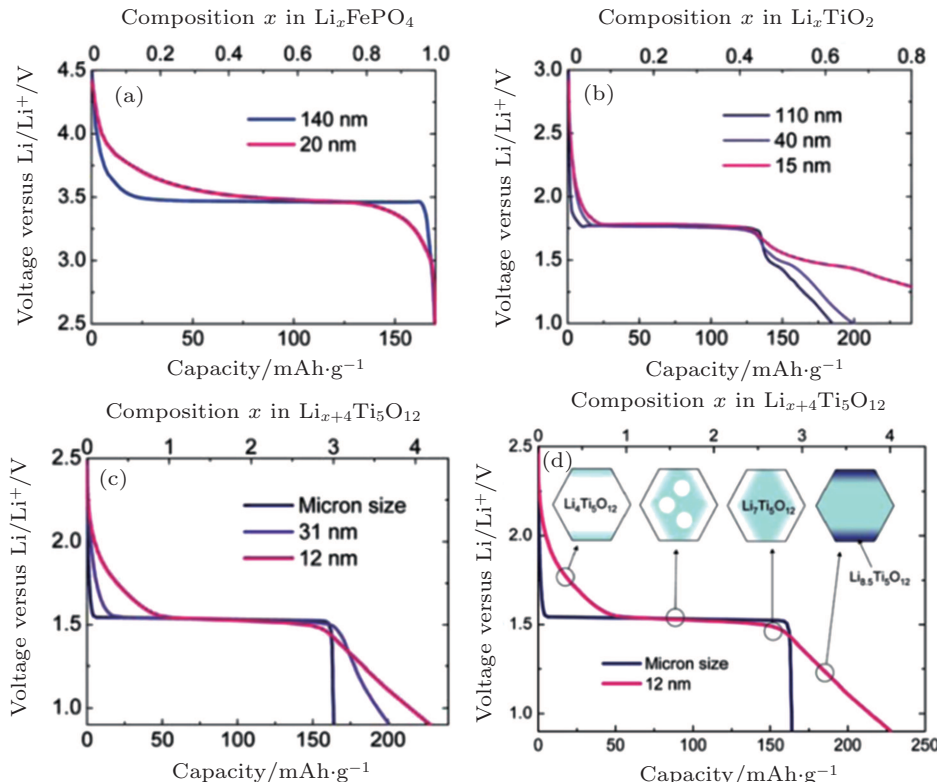


**Fig. 6.** Voltage profiles of different particle sizes for  $\text{Li}_x\text{FePO}_4$  (a), anatase  $\text{Li}_x\text{TiO}_2$  (b), and spinel  $\text{Li}_{x+4}\text{Ti}_5\text{O}_{12}$  ((c) and (d)).<sup>[7]</sup>

When an intermediate phase is stable with lower Gibbs free energy, as shown in Figs. 5(e) and 5(f), it is necessary to consider the two ranges of  $x_1 - x_2$  and  $x_3 - x_4$  respectively, and the explanation is identical to that of phase-separation reaction.

In LIBs, certain ranges of the voltage profile (especially for the low voltage sides) often appear as capacitor behavior. Significantly different from typical voltage profiles for the in-

sertion reaction in Fig. 8(a) and the phase separation reaction in Fig. 8(b), the electric potential changes with the components linearly with a non-zero slope, as shown in Figs. 6(b) and 6(c),<sup>[7]</sup> and Fig. 8(c),<sup>[23]</sup> which usually corresponds to the  $\text{Li}^+$  storage at the interfaces<sup>[23]</sup> or near the surfaces,<sup>[7]</sup> both of which can lead to reconstruction of the surfaces and irreversible capacity loss, although the capacitor-like voltage profiles may just result from the electrolyte decomposition.<sup>[24]</sup>

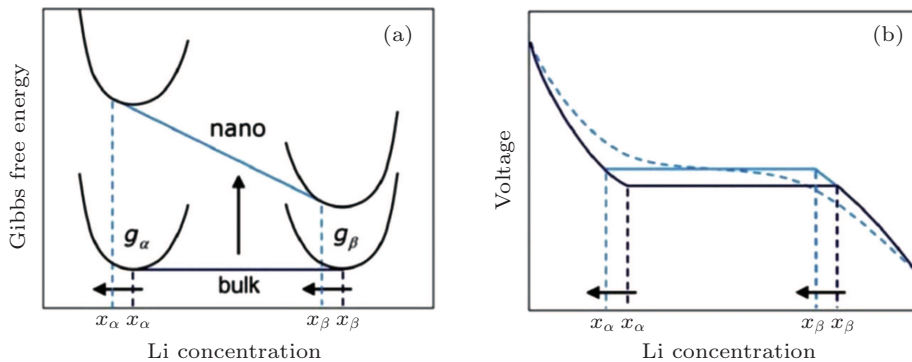


**Fig. 7.** Schematic of the impact of the surface energy on the Gibbs free energy (a) and voltage (b) profile of an insertion material exhibiting a first-order phase transition upon (de)lithiation. A difference in surface energy leads to a different free energy that scales with the particle surface area. The consequences are a change in the chemical potential and hence in voltage plateau and a shift in the solubility limits. A distribution in particle sizes leads to a distribution of voltages as shown by the dotted voltage profile.<sup>[7]</sup>

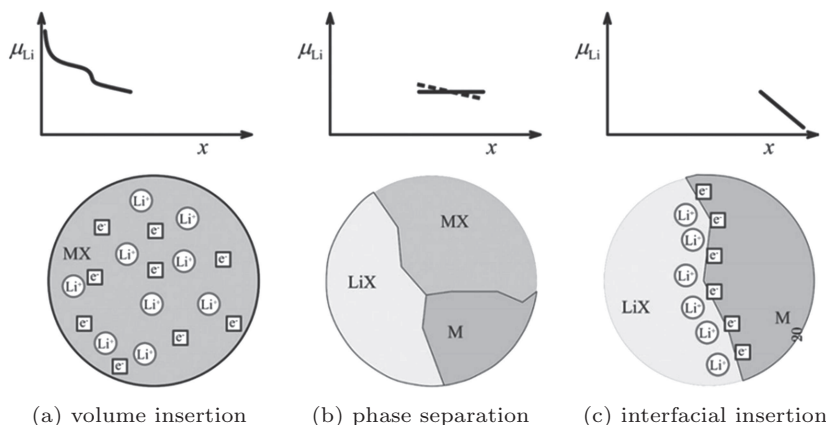


**Fig. 8.** Sequence of three different stages of Li storage. Insertion in the bulk of  $MX$  (a). If the solubility limit is exceeded, a heterogeneous solid-state reaction characterized by phase separation occurs (b). Finally, the interfacial charging takes place (c).<sup>[23]</sup>

#### 4. Spatial distribution of potential in the cell

In order to improve the performance of LIBs, it is necessary to balance the various processes and interactions occurring in electrodes and electrolytes. The temporal-spatial dependent potential in cells is determined together by the Li ions transport in electrodes and electrolytes respectively, as well as by the complicated coupled electrochemical reactions at the interfaces between the electrode and electrolyte. Thermodynamics determines the maximum of power, while the mutual effect of dynamics and mass transfer deviate the system from the ideal thermodynamic equilibrium, influencing the perfor-

mance and cell lifetime. Since multiple transport phenomena are all based on the charges and masses flow, the operating mechanism can be understood from the aspects of electric potential, chemical potential and electrochemical potential. In this way, the limiting factors and their effects on the cell performance can be found to help design batteries with higher capacity, higher power, and longer cycle life.

##### 4.1. The chemical and electronic potential variation within the full circuit

In the batteries, the flows of multiple species and positive/negative charges are often coupled together according

to the Onsager relation, and the mass-charge coupled transport is driven by the concentration related chemical potential (neutral atoms, atomic groups, or vacancies etc.) and electronic potential (electrons or holes). When the electron distribution is considered in the atomic scale, electrons can depart from neutral atoms, for example, the electrons ( $e^-$ ) and lithium ions ( $Li^{+}$ ) can be thought about separately for lithium atoms, then atomic groups or vacancies are left behind (the other charged parts), and they will all re-distribute in the electric field. Then the electric potential describes the gradient distribution of all nonneutral particles, including electrons/holes, nonneutral ions/ionic groups and nonneutral vacancies. In addition, the flow of nonneutral ions, ionic groups or nonneutral vacancies driven by both chemical and electric potential simultaneously, that is, they are actually driven by the electro-

chemical potential.

The operating mechanism in batteries is influenced by coupled electrical and chemical factors, and the whole circuit is powered by the cooperative motion of Li ions and electrons: in the external circuit, the charge transfer is driven by electric potential and mediated through electrons, while in the internal circuit driven by chemical potential through Li ions. However, the charge and mass transfer across the interfaces between electrode and electrolyte is usually of greatest importance in the cells, which is elaborated in the other issue of this series. Simplifying the complicated interphases as the step potential drop because of the existence of space charge layer, the distribution of  $Li^{+}$  chemical potential as well as electronic potential are shown in Fig. 9.

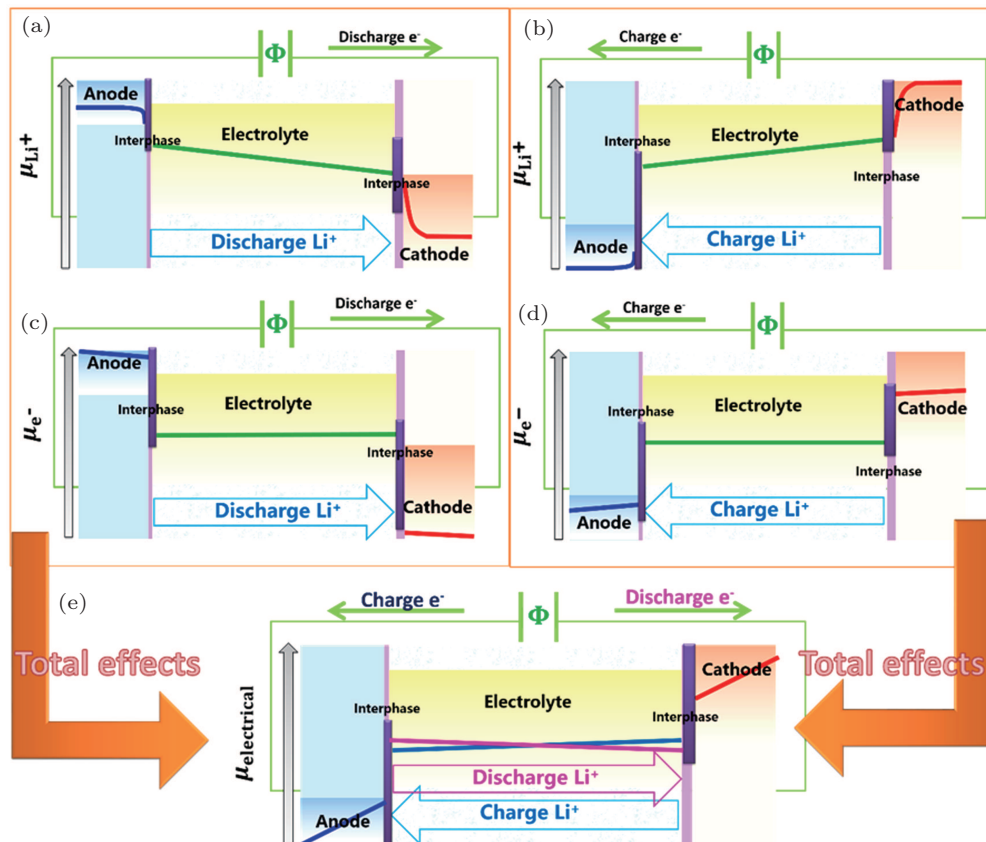


**Fig. 9.** The distribution of lithium chemical potential and electric potential for the whole circuit. (a) The distribution of  $Li^{+}$  chemical potential during the discharge process; (b) the distribution of  $Li^{+}$  chemical potential during the charge process, the contribution of which is opposite to the actual electric potential for the negative charge it has; (c) the distribution of electronic ( $e^-$ ) potential during the discharge process; (d) the distribution of electronic potential during the charge process; (e) the total electric potential distribution of both  $e^-$  and  $Li^{+}$  simultaneously.

Figures 9(a) and 9(b) show the concentration of  $Li^{+}$ , providing the assumption that every effective Li atom (mobile Li atom) has one electron delocalizing from  $Li^{+}$ , and  $Li^{+}$  other than Li is the only mass carrier. The assumption is not always true especially for alloy anodes, which actually comprise itinerant electrons; thus Li ions diffuse accompanied by electrons. The gradient concentration directly results in the chemical potential ( $\mu_{Li^{+}}$ ) variation, which is one of the driving forces. And

the inhomogeneous distribution of nonneutral  $Li^{+}$  also contributes to the electric potential variation, as the other driving force. The sloped line of the electrolyte's potential indicates a nonequilibrium state, and the slope factor is dependent on the current and resistance there, with the assumption that electrons' mobility is negligible when compared to ions' mobility, and all the electric potential change can be attributed only to Li ions' re-distribution during the charge and discharge non-

equilibrium dynamic process.

Figures 9(c) and 9(d) show the other contribution to the redistribution of the electric potential, that is the so-called electronic potential variation defined by the energy of electrons. For electrodes, that is equal to the Fermi energy level, and in electrolyte, that is equivalent everywhere for its electronic insulation, except for regions near the interfaces, where the nonneutral electron or hole defects work.

The total effect resulting from hysteresis is shown in Fig. 9(e), which is consistent with the in-situ electron holography observation of electric potential in an all-solid-state Li-ion battery.<sup>[25,26]</sup> This can be explained as follows: In the charge-discharge process, there usually exists two separately electrochemical half-reactions, which are the so-called electrode reactions. Then the consequent total reaction of the above two half-reactions, namely cell reaction, maintains the electrical neutrality. During the discharge process, when the external circuit is switched on, since the Fermi energy level in an anode is higher than that in a cathode, electrons flow from anode to cathode through the external circuit, while Li ions from anode to cathode through internal section to partly make up for the electrical neutrality of electrodes, leaving behind nonneutral interphases called “space charge layers”. As a result, the electric potential  $\mu_{\text{electrical}}$  distribution is more similar to that of the negative  $\mu_{\text{e}^-}$ , although alleviated by the  $\mu_{\text{Li}^+}$ ’s compensation. In contrast, during the charge process, external electric field makes the mass and charge flows reverse. Note that only the electrons near the Fermi energy level can flow into or out of electrode particles, and the change of Fermi energy level is finite and modulated by the fine crystal structural adjustment. Thus the formation of  $\text{Li}^+$  caused by electrical field induced local phase transition predominately accounts for the

reversed reaction, and electrons flow in the direction opposite of the external circuit to compensate partially for the neutrality. Therefore although theoretical OCV between electrodes can be calculated thermodynamically, the real output voltage must be influenced by dynamic factors such as the above hysteresis effect.

As discussed above, when the current flows through the circuit, the internal resistance in the battery will cause an Ohmic drop, which results in energy loss, also called Ohmic loss. Many factors contribute to the Ohmic drop, including imperfect contact between electrode slurry and metal current collector, welding spot between current collector and external circuit, potential drop on porous electrode with the certain thickness and accordingly the certain resistance, potential drop on the electrolytes (especially for solid electrolytes), and so on. Besides, side reactions often enhance the internal resistance of cell, such as the formation of solid electrolyte interphase (SEI), which is also ascribed to aging.

Another topic with regard to potential is the “overpotential” phenomenon, which is caused by the kinetics of the charge and mass transfer with the response frequencies of 1 kHz and 10 Hz, respectively.<sup>[27]</sup> The Butler-Volmer model has been widely accepted recently to interpret overpotential.<sup>[28]</sup> Besides, other complicated side reactions near or of the electrodes, as shown in Fig. 10,<sup>[29]</sup> have comprehensive influences on the potential distribution adjacent to the region where the reactions occur.

In the following subsections, the factors with less influence on potential distribution, such as separator and current collector, are not focused on. Only the electrode, electrolyte and their interfaces are involved.

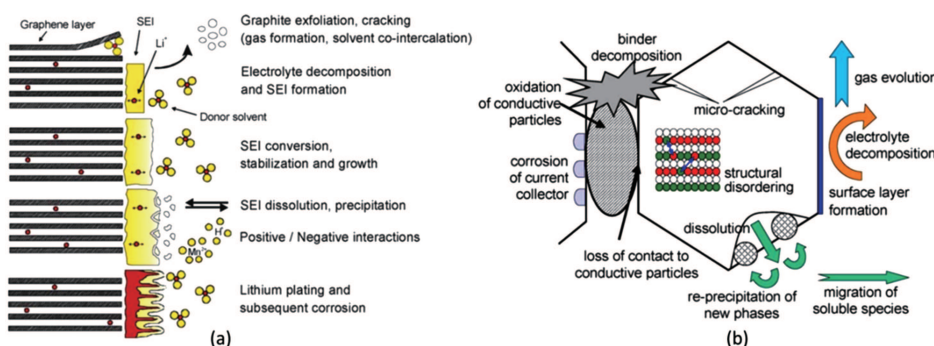


**Fig. 10.** (a) Changes at the anode/electrolyte interface; (b) overview of basic ageing mechanisms of cathode materials.<sup>[29]</sup>

#### 4.2. Hierarchical porous electrodes

Porous electrodes are often designed to be applied to LIBs, and usually contain active materials with sizes ranging from micrometers to nanometers and the conductive additives for lowering the resistance, which are mixed and then spliced by binders as a unit, and electrolyte with high ionic con-

tivity filled into the particles’ skeleton to promote ion diffusion, resulting in a so-called porous electrode shown in Fig. 11. Once there is current in the battery pole pieces with a certain thickness and resistance, the Ohmic drop must occur. For common commercial LIBs, carbon materials are applied as the anodes, which usually have much higher capacity than cathodes.

As a result, the cathode plates are often thicker. Along with the usually lower conductivity (often determined by the conductive additives) of cathode materials,<sup>[30]</sup> the Ohmic drop is more severe accordingly.

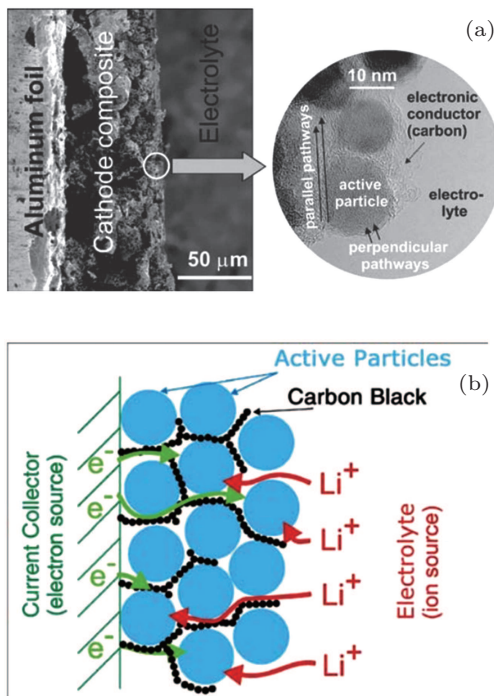


**Fig. 11.** Typical Li ion battery porous electrode. (a) Low magnification (on left) and high magnification (inset on the right). (b) Schematics showing the main phases constituting a modern insertion cathode and its role in transport. The polymeric binder is not shown (its effect on the transport is thought to be marginal).<sup>[31]</sup>

Fine single active particles with size of nanometers to micrometers and the continuous conductive additive ensure high electronic conductivity, so that the active particle surfaces can be seen as an electronic equipotential body. Therefore, the ion transport inside the particle is driven only by the Li concentration gradient (i.e., chemical potential). With high ionic conductivity, the electrolyte can be treated as the equipotential surface of  $\text{Li}^+$  chemical potential, despite the complicated interfaces' space charge layer. Then the Li ion diffusion rate within the active particle becomes the limiting factor of the total diffusion time.

The advantages of small sizes for the active particles are as follows: (i) The diffusion path and grain boundary resistance of every single particle are both reduced to lower the Ohmic drop on the electrode; (ii) In the case of the Li ion transport in the solid host, assuming the diffusion time  $\tau$ , the diffusion length  $L$ , and the diffusion coefficient  $D$ , the relationship among them is:  $\tau = L^2/2D$ , which indicates that a

shorter diffusion path can reduce the diffusion time of  $\text{Li}^+$  and improve the kinetics performance; (iii) As for a fixed total volume of battery pole piece, the smaller size of single particles means a larger reaction area, which can reduce the operating current density per unit area and improve the cathode/anode reaction rate with the given rated current, so as to ameliorate the charge transfer polarization; (iv) Reducing the particle sizes into the order of magnitude of nanometers is a common method to increase the solid solution limit, while simultaneously introducing more defects such as vacancies or interstitials to improve the intrinsic Li ion mobility in the materials. However, nanocrystallization causes some problems, for example: (i) High porosity leads to a suppression of the compact density thus the energy density; (ii) Surface effects predominate over the intrinsic bulk features, which turns the interface resistance into the main limiting factor of the rate performance; (iii) The side effects near the surface increase; (iv) A contact problem appears between the active particles and the conductive additives. Moreover, when the particles size decreases to the order of magnitude of nanometer, other unknown effects may occur, for example: Will the reconstruction of the surface crystal and electronic structures due to the nanocrystallization have the influence the cell performance? Will the nanoscale interface bring about the pseudocapacitive effect or not? What is the formation mechanism of coexistence and segregation of nanoscale phase, or of heterogeneous interface and space charge layer? These are all problems left to be solved.

Given that the size effects are usually accompanied by the interface effects, the problem of the charge and mass transfer across the active particles and electrolytes will be discussed in Section 4.4.

**Table 1.** Relationship between the diffusion coefficient and the particle size.

2D ( $\text{cm}^2/\text{s}$ )	$10^{-14}$	$10^{-12}$	$10^{-10}$	$10^{-8}$	$10^{-6}$	$10^{-4}$
$\sigma/(3.75 \times)$ (S/cm)	$10^{-11}$	$10^{-9}$	$10^{-7}$	$10^{-5}$	$10^{-3}$	$10^{-1}$
$L$ (1 mm)	$10^{12}$	$10^{10}$	$10^8$	$10^6$	$10^4$	$10^2$
100 $\mu\text{m}$	$10^{10}$	$10^8$	$10^6$	$10^4$	$10^2$	1
10 $\mu\text{m}$	$10^8$	$10^6$	$10^4$	$10^2$	1	$10^{-2}$
1 $\mu\text{m}$	$10^6$	$10^4$	$10^2$	1	$10^{-2}$	$10^{-4}$
100 nm	$10^4$	$10^2$	1	$10^{-2}$	$10^{-4}$	$10^{-6}$
10 nm	$10^2$	1	$10^{-2}$	$10^{-4}$	$10^{-6}$	$10^{-8}$
1 nm	1	$10^{-2}$	$10^{-4}$	$10^{-6}$	$10^{-8}$	$10^{-10}$

Table 1 assumes the condition that  $T = 298$  K, and the system is simplified to 1 M dilute solution (the concentration is 1 mol/L) model. The ionic conductivity can be derived from  $\sigma = (Dnq^2)/kT$ ,

$$\sigma(\text{S}/\text{cm})/D(\text{cm}^2/\text{s}) = \frac{nq^2}{kT} = \frac{6.0221415 \times 10^{23} \times 10^3 \times 10^{-6} \text{ cm}^{-3} \times (1.602176565 \times 10^{-19} \text{ C})^2}{1.3806505 \times 10^{-23} \text{ J/K} \times (273.15 + 25) \text{ K}} \\ \approx 3750 \text{ cm}^{-3} \cdot \text{S} \cdot \text{s}.$$

However, since the carrier concentration is unknown, the calculated ratio,  $\sigma/D$ , may be not suitable for the solid electrolytes. The concentration can be estimated from the calculation of defect formation energy, or from the SOC of electrode materials. Thus the above method of estimation is not accurate, and valid values are difficult to directly measure in experiments.

It can be obtained:  $10^2$  s (1.7 min)~ $\sim$ 36 C;  $10^4$  s (2.7 h)  $\sim$  0.36 C. The rate performance between these two points can satisfy the demands of most energy storage devices, so the relationship between the diffusion coefficient and particle size is of importance, as shown in the red and blue square frame. For example, for a particle with a size of about 10  $\mu\text{m}$ , with the requirement for the charge and discharge rate as 1 C, the diffusion coefficient must reach as high as  $3 \times 10^{-9} \text{ cm}^2/\text{s}$ .

### 4.3. Electrolytes

High power density requires fast lithium ion transport. It can be seen from the porous electrode model that lithium ion diffusion path is very short within the electrode particles, resulting in generally small resistance of the battery pole pieces. Therefore, for the traditional battery structure, the potential drop usually lies in the electrolyte section. The high charge and discharge rate usually leads to the energy loss occurring in multiple regions of the cell, among which the significant energy loss and heat generation are usually located on electrolyte.

Electrolyte is the electronic insulator for LIBs, thus only the transport of ions and ionic groups is driven by electrochemical potential. Apart from the interfacial region concerning the space charge layer, it can be considered that the large proportion of the region maintains local charge neutrality. Supposing the thermodynamic equilibrium conditions, the spatial distribution of the lithium concentration is uniform, leading to the equivalent chemical potential everywhere. As a result, the electrochemical potential is equal to the electric potential within the electrolyte. The overall potential drop between the two ends can be simply considered as the Ohmic drop. In comparison with the fluid and mobile electrolytic solution without a boundary, in the case of solid electrolyte with the stable configuration, the strong restrictions of lattices or skeletons may lead to long-range interaction, which can hardly be explained by the general space charge layer model in liquid solution without the specific crystal structure and interacting forces from skeletons. In addition, the Li ion mobility of the solid electrolyte is 1 and electronic conductivity is extremely low. Therefore, a natural question is that as compared with the solvation of Li ions in the electrolytic solution, how can the solid electrolyte maintain the electroneutrality under lattice restriction conditions? To the best of our knowledge, there is little literature presenting investigations of the mass-charge transport model specialized for the crystalline solid electrolytes, which

may depart from the ideal crystal structure with defects and charges.

### 4.4. Interfaces

Providing the two assumptions, i.e., electroneutrality and continuously changing potential, on which the whole discussion is based, a lot of important thermodynamics and kinetics features are focused on the surfaces and interfaces. For example, when overpotential exists, the partial energy dissipates in the form of heat during the charge/discharge process, and the extent of overpotential is related to the charge/discharge rate. The challenging problems about the interfaces that remain to be solved include: (i) the non-linear phenomena resulting from ultrafast charge/discharge, (ii) the space charge layers with distinct characteristics under various conditions, (iii) the pseudo-capacitance effect, (iv) the spatial and temporal scales of the studied objects, (v) the complex side effects and aging mechanism near the interfaces, including the growth of SEI layers, the decomposition of electrolytes, the formation of Li dendrites, the precipitation of transition metals, the existence of the separated interphase between the solid electrolyte and electrode, and so on.

There has been lots of research on the space charge layer in the electrolytic solution. Owing to the difficulties lying in experiments, the establishment of theoretical models and reasonable simulations becomes markedly important. To balance the requirements of accuracy and practicability, the Gouy–Chapman–Stern model is most widely accepted and adopted so far. Based on the space charge layer model and considering the finite rate, the Butler–Volmer model can be used to explain the kinetics factors such as the overpotential, the transfer of species and charge, the irreversible side effects, and so on, which are caused by the difference between the oxidation and reduction rates under the nonequilibrium condition. In addition, the Poisson–Nernst–Planck equation (including modified forms of the PNP equation,<sup>[32,33]</sup>) the classical continuous ion transport model, can be applied to simulate the linear/nonlinear response with the temporal-spatial parameters, to obtain the spatial distribution of the electric potential, charge density and the salt concentration in the electrolytic solution.<sup>[34–36]</sup> The macroscopic continuous model on electric-chemical potential of the solid–liquid interface has been widely studied, including the model based on equilibrium thermodynamics,<sup>[37]</sup> non-equilibrium thermodynamics,<sup>[38]</sup> thermal fluctuations,<sup>[39]</sup> and so on. For the interface between the specific active particle and solvent, both of which have distinct surface structures and chemical properties, the specific theory and simulation at the smaller atoms/molecules scales should be applied to describe the interaction potential among atoms and the electronic structure. For the more complicated phenomena occurring in the practical applications, including the porous electrode geometry,

the small-size effect at the nanometer scale, the wettability of electrolytic solution and the influence of the interfacial strong field effect, more accurate models concerning the quantum and atomistic scales are in demand, followed by the difficulty in balancing the calculation cost and accuracy. Note that unlike the periodic structure of crystalline, the disordered interphases need to be simulated by covering larger structurally spatial scales, while electrode kinetics needs to be simulated by covering wider temporal scales. In addition, in order to predict the materials properties and then realize rational materials design, linking up the simulations at different scales is still a long-term challenge, as well as verifying the theoretical results with relevant experiments.

In the case of electrolytic solution, the investigation of interface is usually based on at least one of two assumptions:<sup>[37–39]</sup> dilute solution hypothesis and local electroneutrality hypothesis. However, the case is different for the solid electrolyte: (i) The dilute solution model does not work for the strong interaction among mobile carriers and between mobile carriers and lattices; (ii) Thermal fluctuation cannot be ignored for the lattice effects; (iii) Given that the chemical potential is almost equivalent all through the inner bulk of the solid electrolytes (which is equal to the charge/discharge current multiplied by the resistance), the chemical potential difference between anode and cathode (which is the so-called OCV when the current approaches 0) drops mainly on the interfaces and causes a sharp concentration change. In this way, the Debye screening length, which is the spatial scale of the space charge layer treated within the classical Debye–Hückel theory, is hard to estimate for the solid materials with the strong interaction and intrinsic lattice stability; (iv) It is a challenge to establish the evolution model of the solid–solid space charge layer, and even the interphases, because of the lack of reliable experimental data and phenomena for establishing the reasonable models. Therefore, the need is most urgent to develop novel characterization techniques combined with multi-scale theoretical models and simulation methods.

## 5. The dependence of voltage on the electrodes

Based on the theoretical derivation above, the OCV of the electrode material can be obtained from the thermodynamics calculation. One available method is to solve the many-body Schrödinger equation with the approximation of density functional theory (DFT) using the electron density as the functional of the ground state energy, aiming at “the energy required to bring all constituent electrons and nuclei together from infinite distance.”<sup>[4]</sup> Combined with the Nernst equation, the reaction energy with Li can be obtained. The DFT calculations are scalable when compared with experiments, and can realize the fast “mapping” of the certain properties of a series of compositions in the phase diagram. The finiteness of Inorganic Crystal Structure Database and Powder Diffraction Database enables

enumerative investigations. When making use of the “elemental substitution” or “machine learning” method,<sup>[41,42]</sup> novel materials and compositions outside the original databases can be built up and studied. So far, applying the high-throughput calculation to screen the high-performance Li ion battery materials has been an important part of the Materials Genome Initiative (MGI). The Li<sup>+</sup> intercalation potential is one of the most easily calculated properties, and Fig. 12 presents the Li<sup>+</sup> intercalation potentials of thousands of materials relative to Li metal.<sup>[40]</sup> The common existing electrode materials and their Li<sup>+</sup> intercalation potentials are summarized in Table 2, grouped by the crystal types.

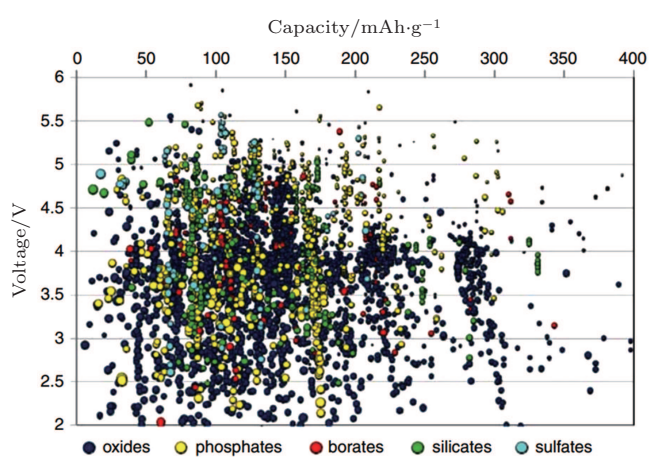


**Fig. 12.** Calculated lithium insertion voltage versus theoretical capacity for several thousand compounds. These compounds have to be further screened on other properties such as Li mobility, electron mobility, stability, and safety before they can be considered reasonable candidates for new battery materials.<sup>[40]</sup>

One of the most important missions for the high-throughput calculation is effective data mining to get the relationship between the crystal structure, composite elements and Li<sup>+</sup> intercalation potential, which is one of the most important scientific bases for screening the possible electrode materials. As shown in Fig. 13, the electrode materials attracting the most extensive attention can be grouped in terms of the intercalation potential as: (i) high-voltage cathodes; (ii) anodes with voltage higher than 1 V that can prevent the SEI or PC/EC decomposition; (iii) anodes with low voltage just above metal Li. The electrodes have been extensively reviewed,<sup>[43–50]</sup> where the common electrolytic solution, whose electrochemical window within the range of 1.0 V–4.3 V, is usually taken into consideration. However, when other electrolytes such as ionic liquid, solid polymer and inorganic solid electrolytes are applied, the range of alternative electrodes can be extended. In addition, the criteria to judge whether the electrodes can be applied to cells are multiple; thus other properties, including Li<sup>+</sup> and electron mobility, stability and the safety of the electrodes operating under given conditions, need to be confirmed by further experiments and calculations.

Table 2. The voltage of common electrodes, relative to Li metal.<sup>[6,49–53]</sup>

	~0 V	0–1 V	1–2 V	2–3 V	3–4 V	4–4.5 V	> 4.5 V
Alloys	Li	Li alloys, graphite/carbons, Si/SiO <sub>x</sub> , Sn/SnO <sub>x</sub> , TCO-1, Si-C, 3M L-20772	Sn-C				
Phosphides		FeP, NiP <sub>2</sub> , NiP <sub>3</sub> , Cu <sub>3</sub> P					
Nitrides		Ni <sub>3</sub> N, Fe <sub>3</sub> N, Co <sub>3</sub> N					
Sulfides		MoS <sub>2</sub> , MnS, CrS	Co <sub>9</sub> S <sub>8</sub> , FeS, Ni <sub>3</sub> S <sub>2</sub> , FeS <sub>2</sub> , NiS, NiS <sub>2</sub> , Cu <sub>2</sub> S, CuS, TiS <sub>2</sub>				
Oxides		MnO <sub>2</sub> , MoO <sub>3</sub> , NiO, FeO, CoO	Co <sub>3</sub> O <sub>4</sub> , CuO, Cu <sub>2</sub> O		MnO <sub>2</sub> , V <sub>2</sub> O <sub>5</sub> , LiV <sub>3</sub> O <sub>8</sub>		
Layered oxides					Li <sub>x</sub> Mn <sub>1-y</sub> M <sub>y</sub> O <sub>2</sub> [M = Cr, Co, ...], Li <sub>1-x</sub> Ni <sub>1-y-z</sub> Co <sub>y</sub> M <sub>z</sub> O <sub>4</sub> [M = Mg, Al, ...]		
Spinel oxides			Li <sub>4</sub> Ti <sub>5</sub> O <sub>12</sub>		LiMn <sub>2</sub> O <sub>4</sub>		
Fluorides	VF <sub>3</sub> , TiF <sub>3</sub>	CrF <sub>3</sub> , NiF <sub>2</sub> , FeF <sub>3</sub>	CoF <sub>2</sub>	CuF <sub>2</sub>			
Borates			LiFeBO <sub>3</sub>				
Silicates			Li <sub>2</sub> FeSiO <sub>4</sub>				
NASICON phosphates		Li <sub>3</sub> TiNb(PO <sub>4</sub> ) <sub>3</sub> , Li <sub>5</sub> V <sub>2</sub> (PO <sub>4</sub> ) <sub>3</sub>	Li <sub>3</sub> TiNb(PO <sub>4</sub> ) <sub>3</sub> , Li <sub>3</sub> Ti <sub>2</sub> (PO <sub>4</sub> ) <sub>3</sub> , Li <sub>4</sub> FeTi(PO <sub>4</sub> ) <sub>3</sub> , Li <sub>5</sub> FeTi(PO <sub>4</sub> ) <sub>3</sub> , Li <sub>5</sub> Fe <sub>2</sub> (PO <sub>4</sub> ) <sub>3</sub>	Li <sub>3</sub> V <sub>2</sub> (PO <sub>4</sub> ) <sub>3</sub>	LiV <sub>2</sub> (PO <sub>4</sub> ) <sub>3</sub>		
Olivine phosphates					LiFePO <sub>4</sub> , Li <sub>1.6</sub> Fe <sub>2/3</sub> PO <sub>4</sub>	LiMnPO <sub>4</sub>	LiCoPO <sub>4</sub> , LiNiPO <sub>4</sub> , LiNiVO <sub>4</sub>
Hydrated phosphates			P-LiFePO <sub>4</sub> · 2H <sub>2</sub> O, S-LiFePO <sub>4</sub> · 2H <sub>2</sub> O, M-LiFePO <sub>4</sub> · 2H <sub>2</sub> O				
Diphosphates and diarsenates		Li <sub>2</sub> VP <sub>2</sub> O <sub>7</sub>	Li <sub>2</sub> FeP <sub>2</sub> O <sub>7</sub> , Li <sub>2</sub> FeAs <sub>2</sub> O <sub>7</sub>	Li <sub>4</sub> Fe <sub>4</sub> (P <sub>2</sub> O <sub>7</sub> ) <sub>3</sub> · 4H <sub>2</sub> O, Li <sub>4</sub> Fe <sub>4</sub> (P <sub>2</sub> O <sub>7</sub> ) <sub>3</sub>	Li <sub>9</sub> V <sub>3</sub> (P <sub>2</sub> O <sub>7</sub> ) <sub>3</sub> (PO <sub>4</sub> ) <sub>2</sub>		LiCrP <sub>2</sub> O <sub>7</sub> , LiMn <sub>2</sub> P <sub>2</sub> O <sub>7</sub> , LiFeP <sub>2</sub> O <sub>7</sub> , LiCoP <sub>2</sub> O <sub>7</sub>
NASICON sulfates			Li <sub>2</sub> V <sub>2</sub> (SO <sub>4</sub> ) <sub>3</sub>	Li <sub>2</sub> Fe <sub>2</sub> (SO <sub>4</sub> ) <sub>3</sub> Li <sub>2</sub> Fe(SO <sub>4</sub> ) <sub>2</sub> Li <sub>2</sub> Fe <sub>2</sub> (MoO <sub>4</sub> ) <sub>3</sub> , Li <sub>2</sub> Fe <sub>2</sub> (WO <sub>4</sub> ) <sub>3</sub> , Li <sub>3</sub> Fe <sub>2</sub> (SO <sub>4</sub> ) <sub>2</sub> PO <sub>4</sub>			
Marinite							
Other NASICON							
Anti-NASICON		Li <sub>5</sub> Fe <sub>2</sub> (PO <sub>4</sub> ) <sub>3</sub> , Li <sub>5</sub> Fe <sub>2</sub> (AsO <sub>4</sub> ) <sub>3</sub>		Li <sub>2</sub> Fe <sub>2</sub> (PO <sub>4</sub> ) <sub>3</sub>			
Fluoro-		Li <sub>2</sub> VPO <sub>4</sub> F	Li <sub>2</sub> FePO <sub>4</sub> F		LiZn <sub>0.1</sub> Fe <sub>0.9</sub> SO <sub>4</sub> F, LiFeSO <sub>4</sub> F, Li <sub>5</sub> V(P <sub>2</sub> O <sub>7</sub> ) <sub>2</sub> F <sub>2</sub>	LiVPO <sub>4</sub> F	LiCoPO <sub>4</sub> F, LiCrPO <sub>4</sub> F, LiMnPO <sub>4</sub> F, LiFePO <sub>4</sub> F
Hydroxy-				Li <sub>2</sub> FePO <sub>4</sub> (OH)	LiFeSO <sub>4</sub> (OH)		LiCoPO <sub>4</sub> OH, LiCrPO <sub>4</sub> OH, LiFePO <sub>4</sub> OH
Oxy-				Li <sub>2</sub> VPO <sub>4</sub> O	Li <sub>5</sub> VO(PO <sub>4</sub> ) <sub>2</sub> Li <sub>2</sub> VO(HPO <sub>4</sub> ) <sub>2</sub> , LiVO(H <sub>2</sub> PO <sub>4</sub> ) <sub>2</sub> , Li <sub>2</sub> VOP <sub>2</sub> O <sub>7</sub> , LiVOAsO <sub>4</sub>		

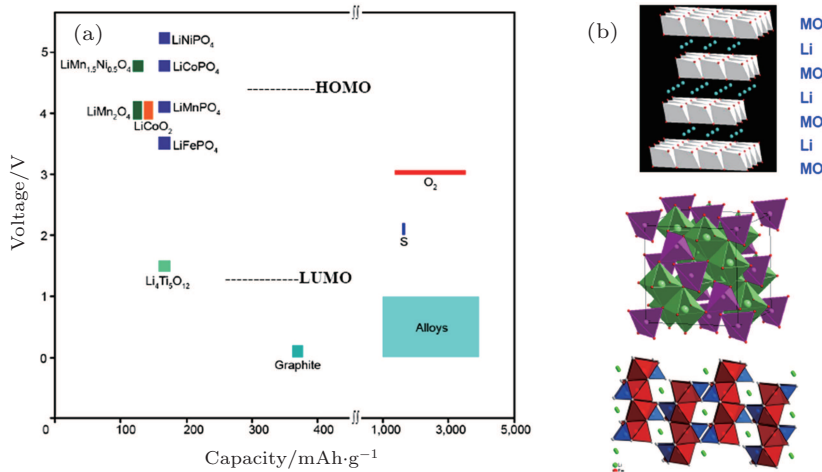


**Fig. 13.** Voltage versus capacity of insertion-compound electrodes (a), and of lithium-alloy anodes and sulfur or oxygen cathodes (b) for a lithium-ion battery. The LUMO and HOMO are for organic liquid-carbonate electrolytes. Oxide structures (top to bottom) are layered  $\text{LiMO}_2$ , spinel  $\text{Li}[\text{M}_2]\text{O}_4$ , and olivine  $\text{LiMPO}_4$ .<sup>[43]</sup>

## 5.1. Elements' influence on OCV

### 5.1.1. Transition metal's influence on $\text{Li}_x\text{M}_y\text{X}_z$

I view of the Fermi energy level explanation of OCV, during the  $\text{Li}^+$  (de)intercalation, the accompanying electron transfer often occurs in 3d atomic orbits of transition metals. As a result, transition metals have an important effect on theoretical  $\text{Li}^+$  intercalation potential. Early investigations indicate that for the layered structure, the materials on the right side of periodic table of elements provide a wider energy gap and higher intercalation potential,<sup>[55]</sup> Al substituted for Co can enhance the intercalation potential.<sup>[56,57]</sup> Early DFT studies based on the single electron approximation without the correction of additional interactions led to a narrower energy gap, which is not quantitatively accurate. However, the qualitative trend of the relationship between intercalation potential and transition metal is offered. Thanks to the correction of calculation methods (including  $+U$  and HSE, to will be discussed below), the accuracy of calculated intercalation potential is greatly improved. In addition, a tremendous amount of information can be derived from the high-throughput calculation, and even from the accessional new data produced by systematic replacement of elements mapped in the periodic table. As an example, figure 12 contains the massive information worthy to be dug into. Figure 14 gives another example, in which the phosphates always provide the higher intercalation potentials than their oxide counterparts (see Fig. 14(a)), whereas figure 14(b) exhibits the various intercalation potentials by varying the transition metals of the phosphate family.<sup>[40,54]</sup>

For  $\text{LiMn}_2\text{O}_4$  with the spinel structure,  $\text{Mn}^{3+} : \text{Mn}^{4+} = 1 : 1$ . The electron configuration of  $\text{Mn}^{3+}$  is  $t_{2g}^3 e_g^1$ , which can result in the Jahn–Teller effects. As a result, with the evolvement of discharge till the proportion of  $\text{Mn}^{3+}$  reaches up to 50%, lattices will distort, leading to a reduction of

cycle performance. One way to avoid the depression is to take advantage of doping methods to reduce the amount of  $\text{Mn}^{3+}$ .<sup>[58–64]</sup> For example, if Mn in  $\text{LiMn}_2\text{O}_4$  is doped by Ni to form  $\text{LiNi}_{0.5}\text{Mn}_{1.5}\text{O}_4$ , during the charge process up to 4.5 V, the 4.1 V plateau arising from  $\text{Mn}^{3+}$  almost disappears. Given that when  $\text{LiNi}_{0.5}\text{Mn}_{1.5}\text{O}_4$  is charged up to 5.0 V,  $\text{Ni}^{2+}$  can be oxidized to  $\text{Ni}^{4+}$ ,  $\text{LiNi}_{0.5}\text{Mn}_{1.5}\text{O}_4$  was found to exhibit another capacity plateau appearing at 4.7 V, called the high voltage cathode by Zhong and Dahn.<sup>[65]</sup> The electrochemical properties of various high voltage spinel cathodes with the different doping elements are listed in Table 3.

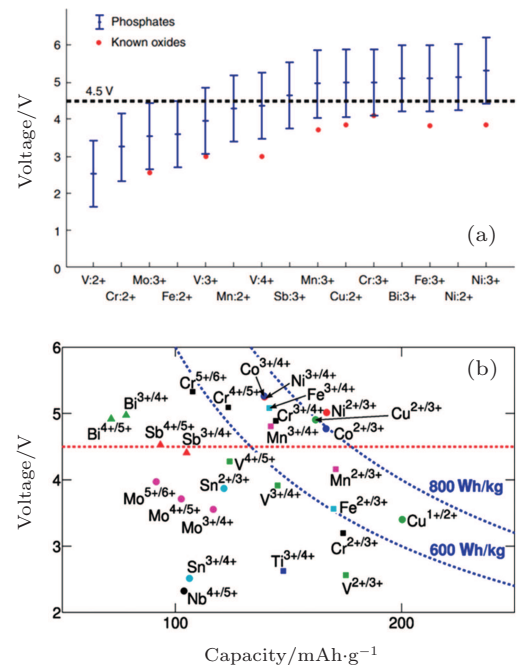


**Fig. 14.** (a) About 450 phosphate compounds, from those in Fig. 12, were used to data-mine the voltage range over which different cations can be oxidized by Li removal.<sup>[40]</sup> (b) Mean voltage in phosphates versus maximum gravimetric capacity achievable.<sup>[54]</sup>

Table 3. Electrochemical data for spinel cathode materials.<sup>[50]</sup>

Cathode material	High-voltage plateau redox couple	Discharge voltage <sup>b</sup> (V versus Li <sup>+</sup> /Li)	Theoretical capacity/mAh·g <sup>-1</sup>
LiMn <sub>2</sub> O <sub>4</sub>	Mn <sup>3+</sup> /4+	4.1	148
LiNi <sub>0.5</sub> Mn <sub>1.5</sub> O <sub>4</sub>	Ni <sup>2+</sup> /4+	4.7	147
LiNi <sub>0.45</sub> Mn <sub>1.45</sub> Cr <sub>0.1</sub> O <sub>4</sub>	Ni <sup>2+</sup> /4+/Cr <sup>3+</sup> /4+	4.7/4.8	145
LiCr <sub>0.5</sub> Mn <sub>1.5</sub> O <sub>4</sub>	Cr <sup>3+</sup> /4+	4.8	149
LiCrMnO <sub>4</sub> <sup>a</sup>	Cr <sup>3+</sup> /4+	4.8	151
LiCu <sub>0.5</sub> Mn <sub>1.5</sub> O <sub>4</sub>	Cu <sup>2+</sup> /4+	4.9	147
LiCoMnO <sub>4</sub> <sup>a</sup>	Co <sup>3+</sup> /4+	5.0	147
LiFeMnO <sub>4</sub> <sup>a</sup>	Fe <sup>3+</sup> /4+	5.1	148

<sup>a</sup>A partial delithiation occurs at ca. 4 V versus Li<sup>+</sup>/Li due to the Mn<sup>3+</sup>/4+ redox couple.

<sup>b</sup>Voltage of the upper plateau.

### 5.1.2. (Poly)anion's influence on Li<sub>x</sub>YM<sub>x</sub>X<sub>z</sub>

For the electrodes, (poly)anions can modulate the redox potentials for transition metals, which has been investigated in NASICON<sup>[67]</sup> and olivine systems (shown in Fig. 15).<sup>[66]</sup> From the aspect of Bronsted acidity, (SO<sub>4</sub>)<sup>2-</sup> > (PO<sub>4</sub>)<sup>3-</sup>,<sup>[67]</sup> while from the aspect of Mulliken electronegativity,

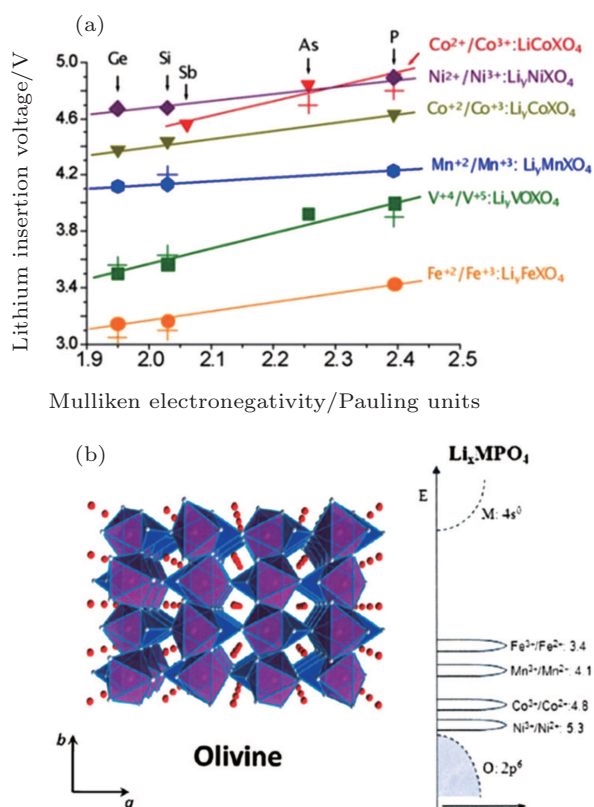


Fig. 15. (a) Calculated and experimental (crosses) lithium insertion voltage for olivine polyoxianionic compounds versus the X Mulliken electronegativity. The lines show the fit to respective linear functions;<sup>[66]</sup> (b) the structure of the ordered olivine.<sup>[46]</sup>

P>As>Sb>Si>Ge.<sup>[66]</sup> Therefore, it can be said that the stronger the electronegativity of central atoms, the stronger the acidity of the polyanionic salts, and the higher the intercalation potential the corresponding electrodes will have. Figure 16 exhibits the multi-electron Li<sup>+</sup> phosphate cathodes made by mixing transition metals with different Y substitution. One advantage is that the substitution of Y with its lower valence can replace the redox couple with one corresponding to higher valences for the transition metals during the charge/discharge, leading to the elevation of output voltage. As in Fig. 16, the intercalation potential of Y = F is higher than that of Y = OH for the stronger electronegativity of F.<sup>[53]</sup> Figure 17 takes Li<sub>x</sub>MPO<sub>4</sub>Y with the tavorite structure as an example. It can be clearly seen that for the same redox couple of the given transition metal the intercalation potential is higher when Y = F than when Y = O or Y = OH.<sup>[49]</sup>

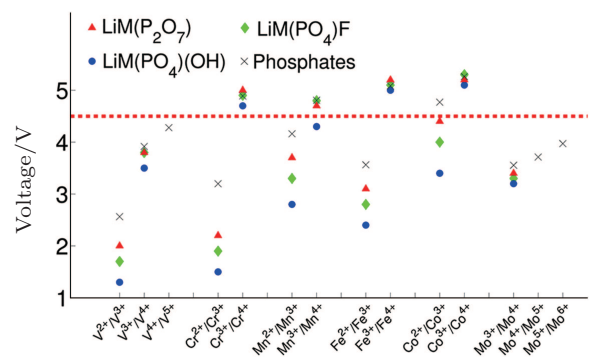


Fig. 16. Computed voltages for different redox couples active in various phosphate and multielectron phosphate cathodes.<sup>[53]</sup>

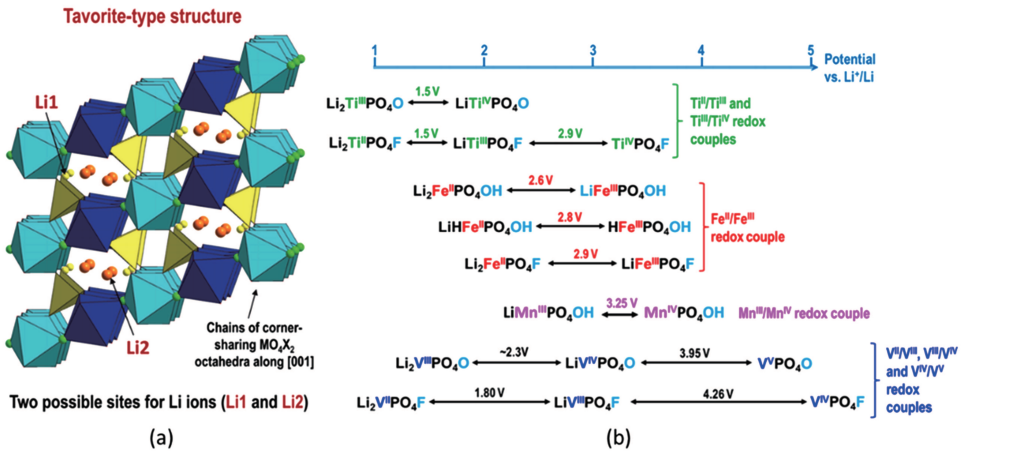


Fig. 17. (a) Representation of the tavorite structural arrangement and (b) overview of corresponding  $\text{Li}_x\text{MPO}_4\text{Y}$  compositions and redox voltages.<sup>[49]</sup>

## 5.2. Structure and order degree influences on OCV

Figure 18 lists the potentials of  $\text{Fe}^{3+}/\text{Fe}^{2+}$  redox couple versus lithium of various Fe-based cathode materials, indicating the strong dependence of the potential on the crystal structure. For the phosphates, complex in solution, sulfates, and others (as listed in Fig. 18), the potential variation span of  $\text{Fe}^{3+}/\text{Fe}^{2+}$  among them is close to 1.5 V. Apart from the influence by the various (poly)anions as discussed in Section 5.1.2, this phenomenon can also be greatly attributed to the differences among structures. In order to discuss the relationship between the electrode potential and structure, we set forth the specialized polymorphism as an example, and then introduce the difference between potentials of two materials with the same components but different structures.

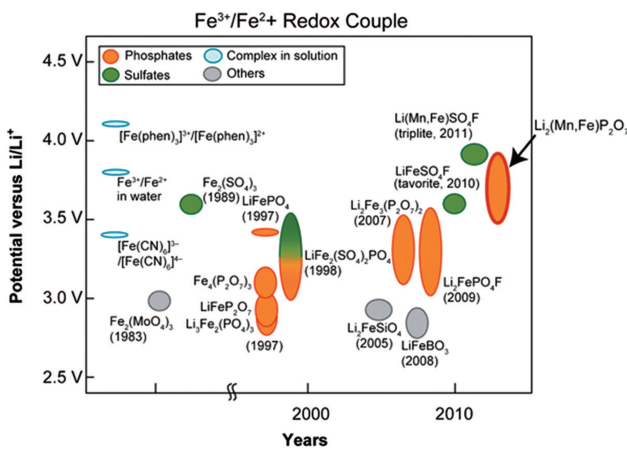


Fig. 18. Historical diagram comparing the potential of  $\text{Fe}^{3+}/\text{Fe}^{2+}$  redox couple (versus  $\text{Li}^+/\text{Li}^0$ ) of various Fe-based (phosphates, sulphates, complexes and others) cathode materials. The Mn-substituted  $\text{Li}_2(\text{Fe}_{1-x}\text{Mn}_x)\text{P}_2\text{O}_7$  binary pyrophosphate shows the highest  $\text{Fe}^{3+}/\text{Fe}^{2+}$  redox potential, close to 4 V and similar to that of  $\text{Li}(\text{Fe}_{1-x}\text{Mn}_x)\text{SO}_4\text{F}$ .<sup>[68,69]</sup>

There are two kinds of crystal structures with different order degree in  $\text{LiNi}_{0.5}\text{Mn}_{1.5}\text{O}_4$ , corresponding to the  $Fdd\bar{3}m$  and  $P4332$  space groups, respectively,<sup>[71]</sup> as shown in

Fig. 19.<sup>[50]</sup> For the  $Fdd\bar{3}m$  structure, Li and O atoms occupy the  $8a$  sites and  $32e$  sites, respectively, and Ni and Mn atoms  $16d$  sites randomly, called the disordered structure, in which the O defects usually occur. While for the  $P4332$  structure, Li atoms occupy  $8c$  sites, Ni  $4a$  sites, Mn  $12d$  sites, and O  $8c$  and  $24e$  sites, called the ordered structure. Figures 20(a) and 20(b)

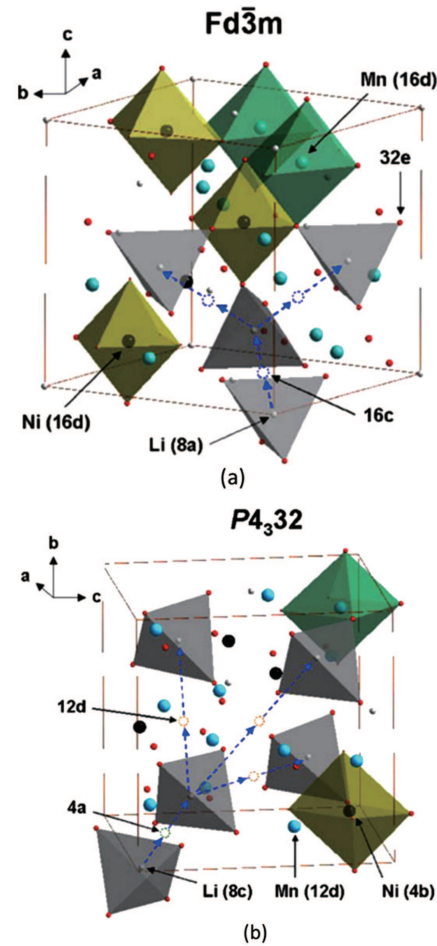
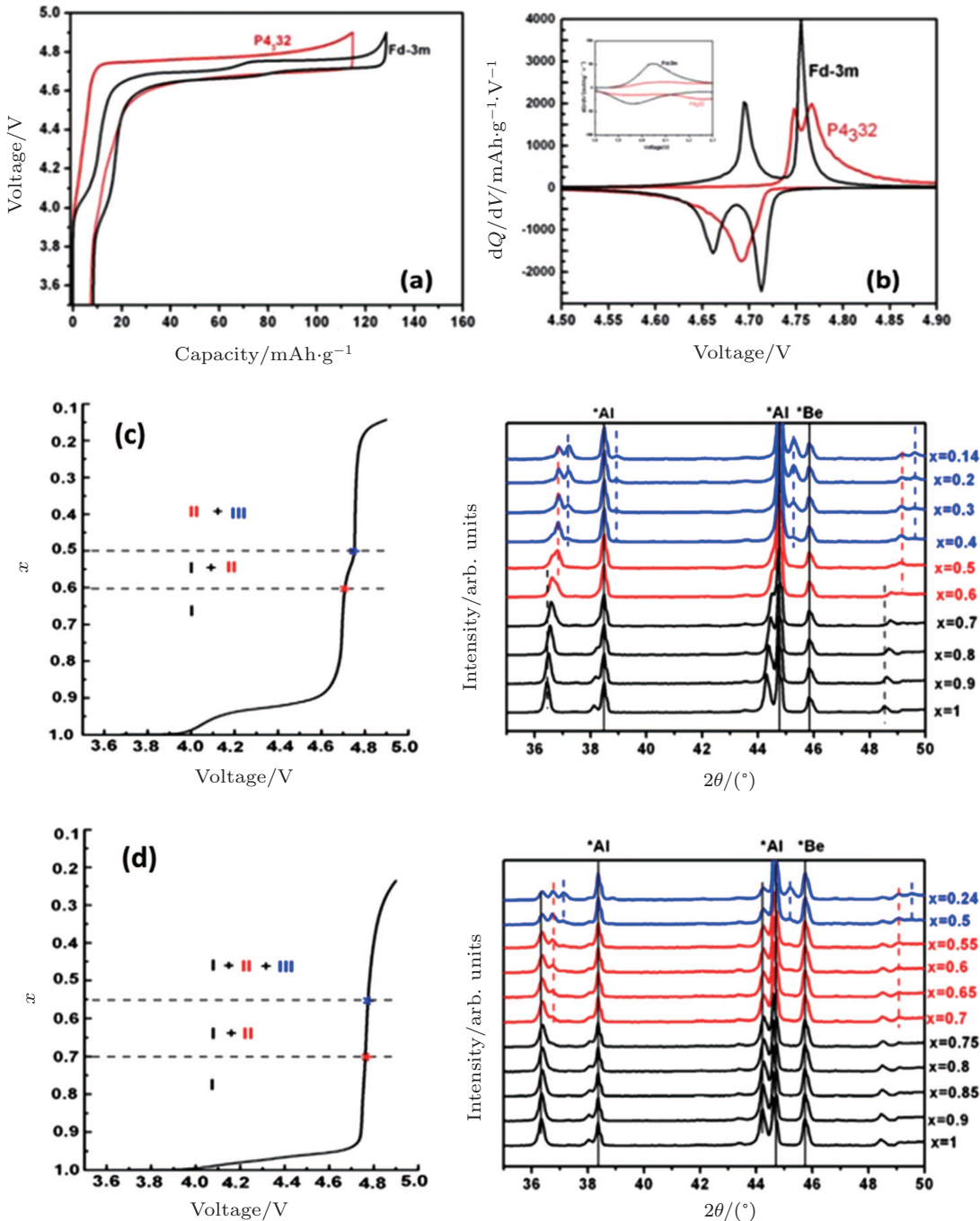


Fig. 19. The structures of  $\text{LiNi}_{0.5}\text{Mn}_{1.5}\text{O}_4$  with the (a)  $Fdd\bar{3}m$  and (b)  $P4332$  space groups.<sup>[50]</sup>

show the electrochemical performances of two structures. In Fig. 20(a), for the  $Fd\bar{3}m$  structure, there is a little capacity in 4.0 V arising from the  $Mn^{3+}$ . In the differential curves in Fig. 20(b), the oxidation peaks of  $Fd\bar{3}m$  lie at 4.69 V and 4.75 V, while those of  $P4_332$  at 4.74 V and 4.77 V, and their reduction peaks of different structures are also different from each other, which can be ascribed to the different band energy structures of different structures. A comparison between the phase transition behaviors of two structures indicates that

during the charge/discharge process, both the  $Fd\bar{3}m$  (lattice parameter: 8.12 Å) and the  $P4_332$  (lattice parameter: 8.16 Å) experience three phase transitions within 3.5–5 V voltage regions, as shown in Figs. 20(c) and 20(d). The investigation of the doping effects on the mechanism and critical points of phase transition for  $LiNi_{0.5}Mn_{1.5}O_4$  is still ongoing. Figure 21 exhibits the polymorphisms of  $Li_2MnSiO_4$ , and the more obvious structural differences contribute to the greater distinction in the calculated average voltages.<sup>[4,72]</sup>



**Fig. 20.** (a) Charge/discharge curves, (b) the corresponding differential capacity versus voltage curves of  $LiNi_{0.5}Mn_{1.5}O_4$  with the  $Fd\bar{3}m$  and  $P4_332$  space groups respectively. The charge curves and XRD spectra of  $LiNi_{0.5}Mn_{1.5}O_4$  with the (c)  $Fd\bar{3}m$  and (d)  $P4_332$  space groups.<sup>[70]</sup>

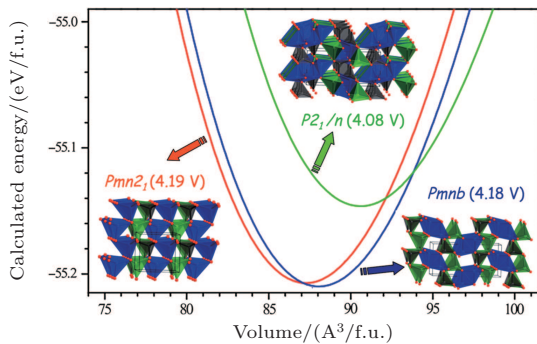


**Fig. 21.** Calculated total energy versus volume curves of  $\text{Li}_2\text{MnSiO}_4$  polymorphs;  $Pmn2_1$  (red),  $Pmnb$  (blue) and  $P2_1/n$  (green). Calculated average voltage for the 2 electron process, host- $\text{Li}_2\text{MnSiO}_4 \leftrightarrow$  host- $\text{MnSiO}_4 + 2\text{Li}$ , is given in parentheses.<sup>[4,72]</sup>

### 5.3. High-voltage cathodes

Generally speaking, the cathode materials with discharge voltage higher than 4.5 V are called the high voltage cathode materials, and they mainly include the spinel, olivine and other polyanionic salts (including  $-\text{O}$ ,  $-\text{F}$ ,  $-\text{OH}$  substitutions). Examples are shown in Table 2, among them, those with the spinel structure, with the olivine structure and with other polyanionic salt structures along with their discharge voltages are shown in Table 3, in Figs. 15 and 16, respectively. The upper limits of the voltage are doubly controlled by both external and internal factors.

The external limiting factor is the highest occupied molecular orbitals (HOMO) of the electrolyte, as shown in Fig. 13, which usually cannot be exceeded by the Fermi energy level of the cathode to prevent the electrolytes from being oxidized during the initial charge/discharge cycles. Methods to mitigate the external limitation include cathode coatings and adding additives contributing to cathodic SEI layers. How-

ever, the elementary way to push the restriction boundary may be the application of electrolytes with wider electrochemical windows, such as the solid electrolytes.

The inner limiting factor lies in the fact that the transition metal elements of the cathodes in the charged state reach a higher valence and exhibit strong oxidizability. As shown from Figs. 22(a)–22(c), the Fermi energy level gradually drops from  $(d+p)^n/d^{n+1}$  close to the primarily  $d$  band of transition metals, into the bottom of the combinational bonding  $(p+d)^n$ , even into anions'  $p$  band. It can be concluded that if the anions prefer to be deprived of the electrons and oxidized, the structure will lose stability during the intensive  $\text{Li}^+$  deintercalation, as shown in Fig. 22(c). As a result, the energy of the redox couple of transition metals should be higher than the  $p$ -orbital level of anions, as shown in Fig. 22(a), or should be close to the  $p$ -orbital level top, which leads to the splitting of  $d$ -orbital level of transition metals into the bonding orbital  $b$ .  $(d+p)^{n+1}$  and anti-bonding orbital  $a$ .  $b$ .  $(d+p)^n$ , and only the electrons of the latter can be deprived during the charge, thus the Fermi energy level can be pinned above the  $p$ -orbital of the anions, as shown in Fig. 22(b). In conclusion, the position of the  $p$ -orbital energy level restricts the voltage of the cathodes intrinsically, which makes it necessary in materials design to match the energy level of the redox couples of transition metals and the  $p$ -orbital of the anions. In the early Li secondary batteries, sulfides such as  $\text{LiTiS}_2$ <sup>[73]</sup> are used as the cathodes. However, the energy level of the high oxidation state of transition metals is lower than the  $3p$ -orbital level of S, resulting in the preferential oxidation of S ions and the low OCV. Oxygen has lower energy with  $2p$ -orbital than S with  $3p$ -orbital and promises a higher OCV versus given anode, thus oxide cathodes are much more widely applied than sulfide ones.

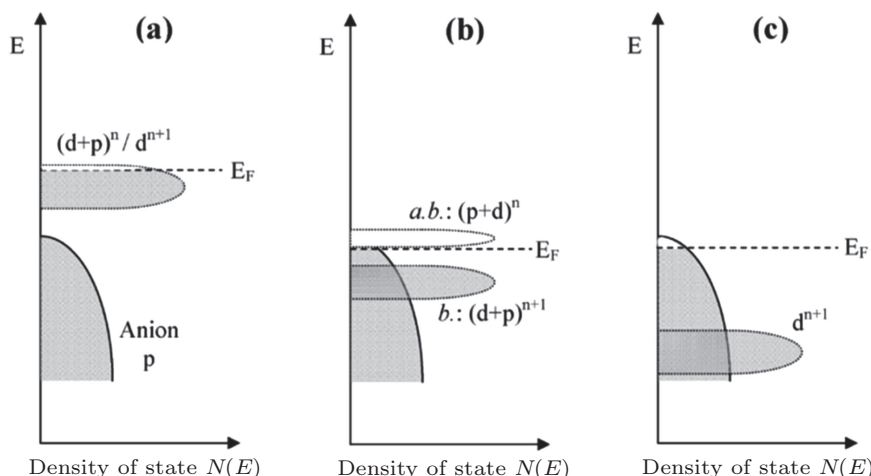


**Fig. 22.** Schematic representation of a slightly oxidized redox couple for different positions relative to the top of the anion  $p$  bands. (a) Itinerant versus polaronic character of hole states of a couple on the approach to the top of the anion  $p$  band, (b) pinned couple with predominantly antibonding (a.b.) anion  $p$  hole states and predominantly cation bonding (b.) states, and (c) couple too far below top of anion  $p$  band for significant cation  $d$  character in hole states.<sup>[44]</sup>

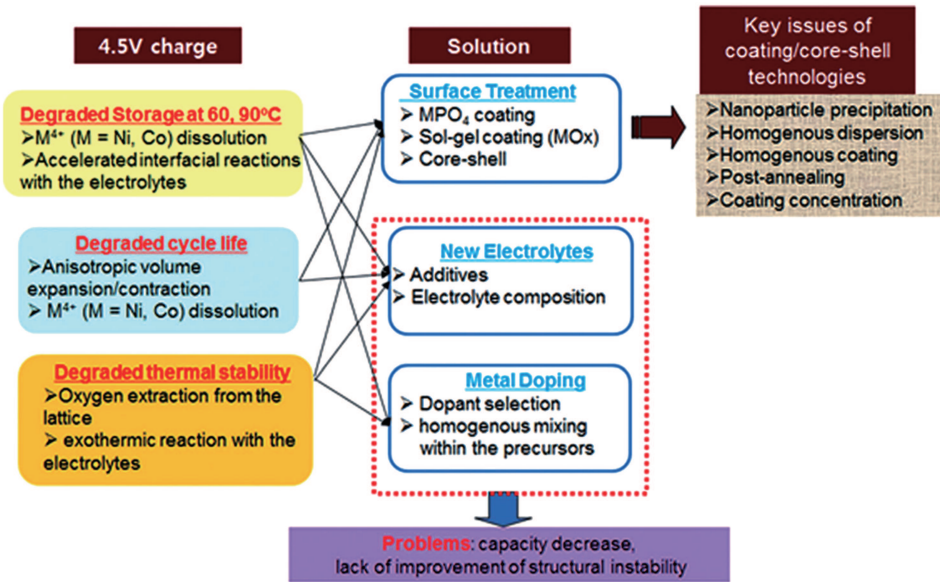


Fig. 23. Problems and their solutions for cathode materials under increasing operating voltages and temperatures.<sup>[74]</sup>

When the layered cathodes Li[Ni<sub>x</sub>Co<sub>y</sub>]O<sub>2</sub> are highly charged, the O 2p-orbital usually tends to lose electrons rather than the transition metal 3d-orbital. In other words, the O<sup>2-</sup> is oxidized by the high-valent transition metals<sup>[75]</sup> and may be released in the form of O<sub>2</sub>,<sup>[76,77]</sup> making the lattice structure lose its stability and causing safety problems. Manganese doping can lower the energy level of O<sub>2</sub> p-orbital and enhance the thermal stability, at the cost of the capacity decreasing.<sup>[77]</sup> Apart from the instability arising from O<sub>2</sub> evolution, other problems related to the layered cathodes and their promising solutions are summed up in Fig. 23.<sup>[74]</sup>

The more fundamental method to improve stability is to screen for novel materials with the proper structures and compositions that promise higher thermal stability. For example, the spinel structure material Li[Ni<sub>0.5</sub>Mn<sub>1.5</sub>]O<sub>4</sub> has higher thermal stability than the layered materials. Figure 24 shows the relationship between the output voltage (i.e., intercalation potential) and the oxygen chemical potential for thousands of materials, obtained from high-throughput calculations. With the chemical potential depicted by the scatter diagram, the charged cathode (under the high intercalation potential) with higher valent transition metal has the probability to decompose, the products can be thermodynamically O<sub>2</sub> (if the charged state oxygen chemical potential is above 0 eV versus O<sub>2</sub>) along with other phases containing the same transition metal with the lower valence (to keep the products' electric neutrality). This trend can be seen: the materials with higher intercalation potential usually have higher O chemical potential. Moreover, the safety range of the O chemical potential determines the upper limits of the voltages of the cathodes. However, as shown in Fig. 24, corresponding to the same intercalation potential, the range of O chemical potential is very

wide, enabling the possibility of materials design for high-voltage and high-stability cathodes. Although the phosphates are widely believed to have higher stability even when charged to a higher voltage, it can be inferred from the calculated results that borates and silicates may perform better, guiding the direction for further material screening and design.<sup>[40]</sup>

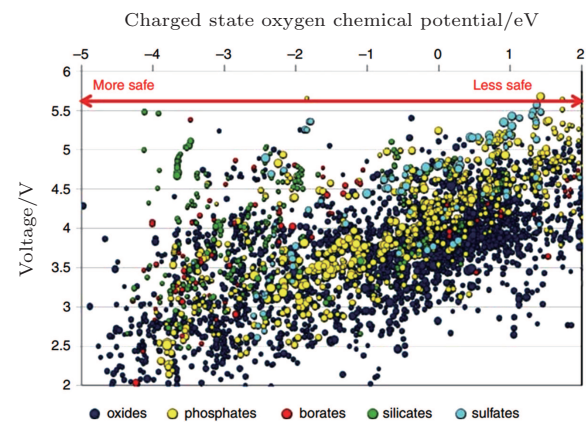


Fig. 24. Oxygen chemical potentials at which the charged state of thousands of cathode materials decompose versus their Li intercalation voltage. A more negative chemical potential indicates that the material can better withstand a reducing environment (higher temperature) and hence is safer.<sup>[40]</sup>

#### 5.4. Anodes

Since OCV is the difference between the anodic and cathodic Li ion chemical potentials, or from the other aspect, between their electronic Fermi energy levels (i.e., their electric potentials), higher OCV can theoretically be obtained by lowering the (de)lithiation potential of the anode. Given that Li metal has the most negative standard electrode potential among the metals, it can be applied as the anode with the lowest potential for Li secondary batteries, as shown in Table 2.

However, when the output voltage of the anode is lower than 1 V versus Li metal anode, as shown in Fig. 13,<sup>[43]</sup> the Fermi energy level of the anode will be lower than the lowest unoccupied molecular orbital (LUMO) of organic electrolytic solutions, which makes the electrolytes decompose and SEI layers form. Note that since the current batteries are always assembled in the fully discharged state, and cathodes are usually the only Li source, then the formation of SEI layer will consume Li ions of the cathodes and lead to capacity loss.

Usually, ethylene carbonate (EC) can be added to the electrolyte to form a stable SEI layer during the initial cycles. Thanks to the additives, graphite with the potential of 0.2 V can be applied as the anode for the batteries, with low irreversible capacity loss. In addition, the not too low potential also avoids the Li plating. With other advantages, such as the low cost and plentiful raw materials, high specific (2.5 times more than  $\text{LiCoO}_2$ ) and volumetric (nearly equal to  $\text{LiCoO}_2$ ) capacities, low voltage hysteresis, good rate capability, good thermal stability (providing the not too large surface), low volume expansion during lithiation, long cycle life, high Coulombic efficiency (CE), good electronic conductivity, good compaction performance, and so on, graphite anodes are called “miracles”.<sup>[6]</sup>

In order to obtain the higher capacity, Li alloy anodes (including metal oxides sharing the same mechanism with alloys) are widely investigated.<sup>[6]</sup> Since their Fermi energy levels are less than 1 eV versus Li metal, it is a challenge to enable the formation of SEI layer at the initial cycles (the better solution is to complete the formation of SEL layer before the batteries are assembled) and handle the capacity loss. In addition, the volume expansion during the lithiation (charge) process is usually a serious problem. Moreover, for the Li alloy anodes with low potential, Li plating on the surface of SEI layers should be avoided because it can bring about the safety issues, lead to the continuous growth of SEI layers and capacity loss.

The problems related to the low potential anodes can be solved by the application of electrolytes with a wider electrochemical window and higher stability. Another solution is to take advantage of anodes with potential higher than 1 V, such as  $\text{Li}_4\text{Ti}_5\text{O}_{12}$ , so that the electrolyte decomposition and the SEI layer growth can be prevented within the operating voltage. In addition, the higher potential avoids Li plating, has the zero-strain property, and high rate capability.

## 5.5. High-capacity electrodes and conversion reactions

For the traditional electrodes based on the intercalation reaction (e.g.,  $\text{LiCoO}_2$  and  $\text{LiMn}_2\text{O}_4$ ) or phase transition (e.g.,  $\text{LiFePO}_4$  and  $\text{Li}_4\text{Ti}_5\text{O}_{12}$ ),<sup>[9]</sup> the specific capacity is usually restricted by the electron exchange capacity on the  $3d$ -orbital of transition metals. In 2000, Poizot *et al.* found the novel reversible Li storage mechanism in the transition metal

oxides,<sup>[78]</sup> followed by the discovery of abundant transition metal sulfides, fluorides, nitrides and phosphides with the similar mechanism,<sup>[8,79–87]</sup> which reads:  $MX + \text{Li} \leftrightarrow \text{Li}X + M$  ( $X = \text{O}, \text{S}, \text{F}, \text{N}, \text{P}, \text{Se}; M = \text{Ti}, \text{V}, \text{Cr}, \text{Mn}, \text{Fe}, \text{Co}, \text{Ni}, \text{Cu}, \text{Zn}, \text{Sn}, \text{Sb}, \text{Ru}, \text{Mo}$ ), called the conversion reaction. Based on this mechanism, there can be more than one oxidation state of the transition metal’s redox couples, and the Li storage capacity can be increased to 400–1100 mAh/g. The average OCV (AOCV) can be calculated from the thermodynamic data once the cathode and anode are chosen.<sup>[8,80]</sup> In 2011, Zu and Li calculated the AOCVs of the binary transition metal compounds with different anions ( $X = \text{F}^-, \text{O}^{2-}, \text{S}^{2-}, \text{N}^{3-}$ ), versus the various metallic anodes (Li, Na, Mg, Al), as shown in Fig. 25.<sup>[9]</sup> With a simple calculation method based only on the known thermodynamic data, the Li-, Na-, Mg-, Al-, Zn-based batteries’ conversion reactions can be systematically investigated, aiming at screening for secondary batteries with higher energy densities.

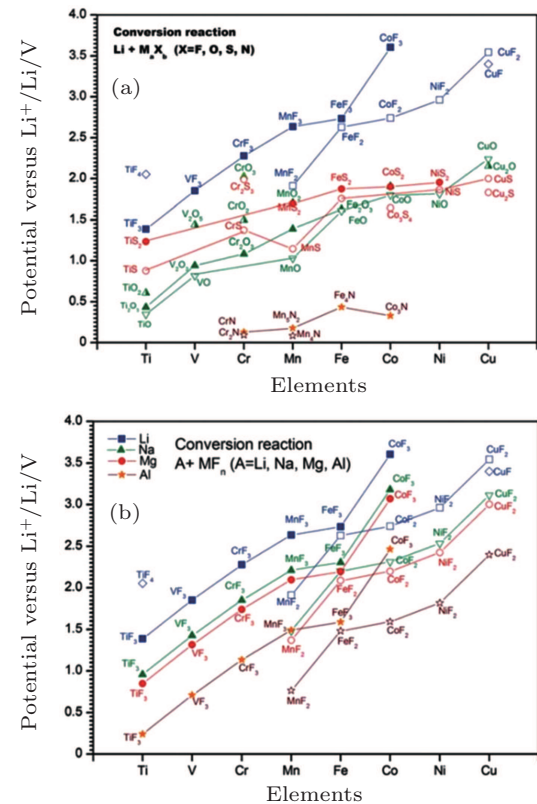


**Fig. 25.** Calculated EMF values ( $V$ ) of conversion reactions between (a) selected binary transition metal compounds and lithium, (b) selected binary transitional metal fluorides and Li, Na, Mg, or Al.<sup>[9]</sup>

## 6. Deviation from the theoretical calculation

As reviewed in Section 3, the OCV can be calculated from the aspect of electronic Fermi energy level or the Li chemical potential. As for the Fermi energy level aspect, the problems concerning the electronic structure are as follows:<sup>[4]</sup> (i) The actual energy band is not exactly derived from the rigid band model, and the Li insertion during the discharge has an impact

on the crystalline structure and thus on the electronic structure of the host matrix. (ii) The electrons may not totally transfer to or from the host matrix; instead, they may interact with  $\text{Li}^+$ , or to say, electrons may not completely delocalize from Li atoms. (iii) The electrons may also not only transfer to the expected transition metal's redox couples, as shown in Fig. 3, but also partly to the anions or anionic groups, as shown in Fig. 22(b). Given the above problems, the voltage profile is hard to obtain from the aspect of Fermi energy level.

A more practical method is to calculate the total free energies of both host compound and Li metal, as explained in Eq. (3), resulting in the OCV versus Li metal anode. Since

$$\Delta G_r = \Delta E_r + P\Delta V_r - T\Delta S_r, \quad (5)$$

where  $\Delta S_r$  or  $\Delta V_r$  usually has an ignorable effect on the cell voltage ( $< 0.01$  V),  $\Delta G_r$  can be approximated by the internal energy  $\Delta G_r$ . In this way, DFT calculation can be applied to obtain the ground-state energies at 0 K.

### 6.1. Thermodynamics: Deviation from the ideal structure<sup>[4]</sup>

DFT calculation can be applied to investigate the periodic crystals with high accuracy, although for the electrodes in reality at the specific SOC, the Li ions and vacancies are usually distributed in a certain random degree. For the partially disordered crystals, the long- or short-range order of Li ions will make a difference to the actual voltage profile, so, only the SOC with the well-known Li ions distribution can be calculated. Even with the help of cluster expansion, only a few states can be established, and their free energies at 0 K have been calculated, as shown in Fig. 26(a). In addition, the disorder effect in the crystal caused by defects or mixing also shifts

the voltage profile as shown in Figs. 26(a) and 26(b). Moreover, the calculations for the disordered structures are often imposed to start from an ordered simplified structure (for example, supercells are introduced to simulate the crystal with defects, and the adopted supercell is endowed with the periodicity), which leads to deviation from the reality.

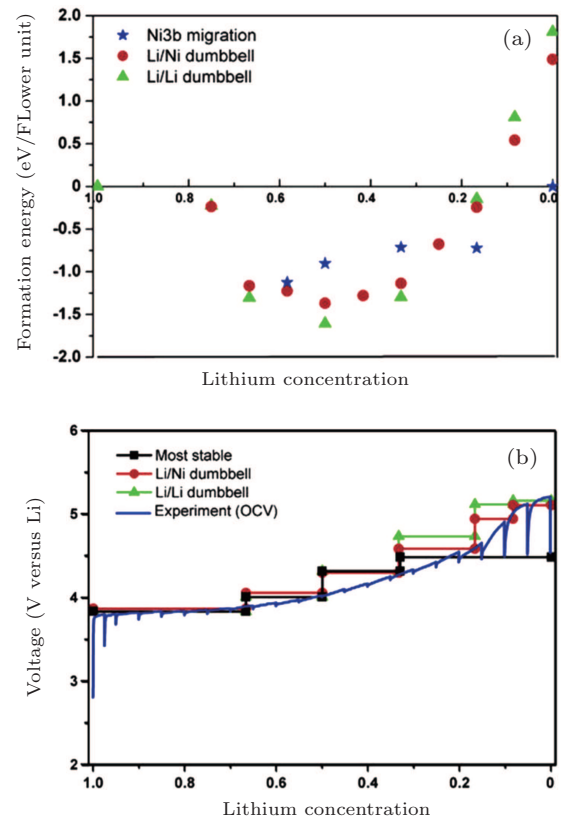


**Fig. 26.** For  $\text{LiNi}_{0.5}\text{Mn}_{0.5}\text{O}_2$ : (a) formation energy as a function of Li concentration of structures with three different lithium/nickel configurations. (b) Comparison between the calculated and experimental voltage curves.<sup>[88]</sup>

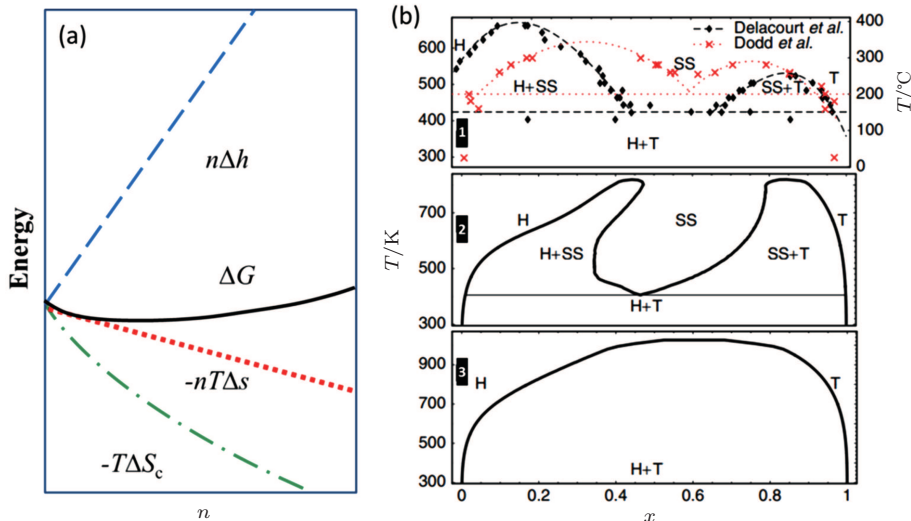


**Fig. 27.** (a) The deviation from ideal crystallographic structure contributed by finite temperature induced entropy changing; (b)  $\text{Li}_x\text{FePO}_4$  phase diagram: experimental phase boundary data (top panel) taken from Delacourt et al.<sup>[89]</sup> and from Dodd et al.;<sup>[90]</sup> calculated (middle panel) with both Li and electron degrees of freedom and (bottom panel) with explicit Li only.<sup>[91]</sup>

At finite temperature above 0 K, entropy should be accounted for, as shown in Fig. 27(a), which can stabilize the structure. In some cases, considering only the configurational ionic entropy is not enough to reproduce the experimental results. Taking LiFePO<sub>4</sub> as an example, as shown in the top panel of Fig. 27(b) for the experimental result and the bottom panel of Fig. 27 for the computed one. Therefore, the configurational electronic entropy should be included; the corresponding result in the middle panel of Fig. 27(b) is consistent with the experimental one. Besides, other complicated phenomena, such as the nano-size effects and interphase effects, are still challenging.

## 6.2. Kinetics: Non-equilibrium asymmetric reaction path

An obvious hysteresis usually occurs in the conversion reaction, which can be ascribed to kinetics, including the simultaneous displacement of inserted Li ions and host matrix ions both, and the existence of nano-particles with the large specific surface areas after the initial cycles.<sup>[78,80,92]</sup> Besides, Li-storage obeying the conversion mechanism is often accompanied by complicated phenomena such as phase separation and interphase Li storage, rather than merely Li insertion, as shown in Fig. 8.<sup>[23]</sup>

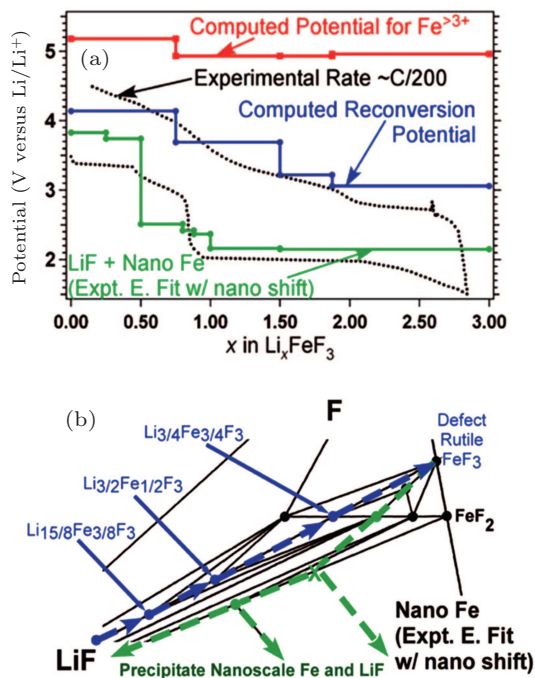


**Fig. 28.** (a) The voltage profile for iron fluoride reconversion during charging (blue, solid line) as compared with the voltage profile for iron fluoride conversion when accounting for the energy of GGA computed nanoscale Fe (green, solid line) and the experimental profile (black, dotted line). The potentials required to form phases with Fe><sup>3+</sup> during reconversion (red, solid line) are also presented. (b) The corresponding reaction path is highlighted for discharge (green, dashed arrows) and charge (blue, dashed arrows).<sup>[93]</sup>

As for Li<sub>x</sub>FeF<sub>3</sub>,<sup>[93]</sup> the voltage profile is shown in green line in Fig. 28(a) and the corresponding discharging reaction path is shown in green dashed line in Fig. 28(b). However,

the charging reaction path shown in blue dashed line is not consistent with that in green dashed line, and neither is the voltage profile. The phenomenon of non-equilibrium asymmetric reaction paths, as well as the corresponding significant polarization and the consequent considerable hysteresis of voltage profile for the conversion (discharge) and reconversion (charge), can be explained by kinetic models, based on the fact that the diffusion coefficient of Li<sup>+</sup> is much larger than that of Fe. In the conversion process, the interdiffusion problem can be thought as follows: at low temperatures, structures often convert to the reaction product that is kinetically most easily reached, rather than to the thermodynamic ground state. In the conversion reaction beginning with Li and FeF<sub>3</sub>, because of the of Fe having lower diffusivity than Li, Fe<sup>3+</sup> tends to be reduced to Fe<sup>2+</sup> rather than metallic Fe nano-particles to compensate for the fast loss of Li<sup>+</sup>, resulting in thermodynamically unstable products. For similar reasons, in the reconversion reaction beginning with Fe and LiF, because of the Fe-deficiency ascribed to the slower diffusivity, the Fe tends to be oxidized to Fe<sup>3+</sup>, resulting in stable products, including Li<sub>3/4</sub>Fe<sub>3/4</sub>F<sub>3</sub>, Li<sub>3/2</sub>Fe<sub>1/2</sub>F<sub>3</sub>, Li<sub>15/8</sub>Fe<sub>3/8</sub>F<sub>3</sub>.

## 6.3. The correction of the calculation methods<sup>[94]</sup>

With the local density approximation (LDA) and the generalized gradient approximation (GGA) of exchange-correlation potential within the DFT framework,<sup>[95–97]</sup> early computational studies of cathodes usually underestimated the band gaps, corresponding to the underestimation of the theoretical OCV. This is due to the self-interaction error, and can be explained from the nature of Kohn–Sham formulation, in which the energy is obtained by solving the one-electron equation written as

$$\left[ -\frac{\hbar^2}{2m} \nabla^2 + V(\mathbf{r}) + V_H(\mathbf{r}) + V_{XC}(\mathbf{r}) \right] \psi_i(\mathbf{r}) = \epsilon_i \psi_i(\mathbf{r}), \quad (6)$$

where the first term is the kinetic energy of the electron, the second is the potential energy of an electron interacting with the nucleus,  $V_H$  is the Hartree electron–electron repulsion potential, and  $V_{XC}$  is the exchange–correlation potential. In this way, all the electron–electron interactions are grouped into the Hartree term, while others are grouped into the exchange–correlation term. The Hartree potential reads

$$V_H(\mathbf{r}) = e^2 \int \frac{n(\mathbf{r}')}{|\mathbf{r}-\mathbf{r}'|} d^3 r'. \quad (7)$$

The above formula describes the Coulombic interactions between the electron and the total electron density of the system. Note that the total density contains the electron’s repulsion to itself, which is unphysical and gives rise to the self-interaction error (SIE). In order to minimize the self-interaction, the unpaired electrons tend to delocalize in real space. However, as pointed out by Zhou *et al.*,<sup>[98]</sup> for cathodes with the transition metals, the partially filled 3d-shell electrons tend to interact

with each other and consequently to be localized. DFT+U introduces a single numerical parameter  $U-J$  to correct the electron self-interaction, and a voltage profile coinciding with experimental result can be obtained, as shown in Fig. 29.

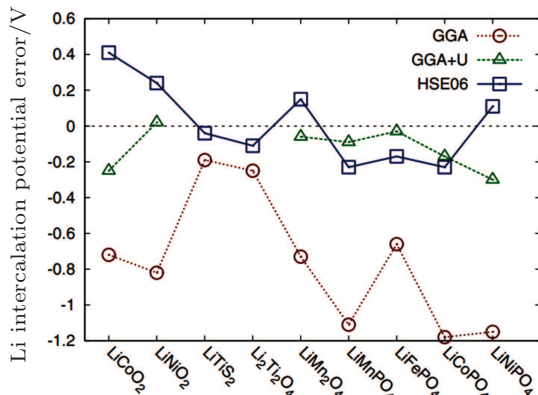


Fig. 29. Error in calculated Li-insertion voltages for a series of cathode materials using the standard GGA, GGA+U, and HSE approximation.<sup>[99]</sup>

The shortcoming of the above method lies in the adjustable parameter  $U-J$ , which should be provided by referring to the experiments or other separate calculations. Another method to correct the potential calculation is to mix exact Hartree–Fock (HF) exchange energy with DFT to get rid of other parameters, called the hybrid functional. However, the exact exchange introduced by HF method is nonlocal, which increases the calculation costs greatly (for 50–100 times more calculating time). Since the exchange interaction involves long- and short-range, Heyd–Scuseria–Ernzerhof (HSE) introduces the HF exchange only to the short range part, which can give the result in accordance with the experiment within the acceptable calculation costs as shown in Fig. 29.<sup>[40]</sup>

## 7. Conclusion

This review introduces the relationship among the electric potential, chemical potential, electrochemical potential, and the Fermi energy level in lithium ion batteries, as well as the relationship between the OCV and the structure, as well as the potential distribution all through the whole cell. A better understanding of the above scientific problems contributes to developing and designing high voltage cathodes, to designing interfaces to reduce the Ohmic drop of the internal circuit, to mitigating the heat generation during operation to prolong service life, to improving the rate performance, to retarding the interfacial ageing, to prolonging cycle life at a high rate, and so on. The internal circuit's potential usually drops at the interfaces, determining the output voltage and power density and structural stability, although it is still a great challenge to investigate the thermodynamic and kinetic processes at the interfaces either experimentally or theoretically.

## References

- [1] Li J, Ma C, Chi M, Liang C and Dudney N J 2015 *Adv. Energy Mater.* **5**
- [2] Baggetto L, Niessen R A H, Roozeboom F and Notten P H L 2008 *Adv. Funct. Mater.* **18** 1057
- [3] Palacin M R 2009 *Chem. Soc. Rev.* **38** 2565
- [4] Meng Y S and Arroyo-de Dompablo M E 2009 *Energy Environ. Sci.* **2** 589
- [5] Owen J R 1997 *Chem. Soc. Rev.* **26** 259
- [6] Obrovac M N and Chevrier V L 2014 *Chem. Rev.* **114** 11444
- [7] Wagemaker M and Mulder F M 2013 *Accounts Chem. Res.* **46** 1206
- [8] Li H, Balaya P and Maier J J 2004 *Electrochim. Soc.* **151** A1878
- [9] Zu C X and Li H 2011 *Energy Environ. Sci.* **4** 2614
- [10] Dahn J R 1991 *Phys. Rev. B* **44** 9170
- [11] van der Marel C, Vinke G J B and van der Lugt W 1985 *Solid State Commun.* **54** 917
- [12] Wu H and Cui Y 2012 *Nano Today* **7** 414
- [13] van der Ven A, Garikipati K, Kim S and Wagemaker M J 2009 *Electrochim. Soc.* **156** A949
- [14] van der Ven A, Bhattacharya J and Belak A A 2013 *Accounts Chem. Res.* **46** 1216
- [15] Kobayashi G, Nishimura S I, Park M S, Kanno R, Yashima M, Ida T and Yamada A 2009 *Adv. Funct. Mater.* **19** 395
- [16] Burch D and Bazant M Z 2009 *Nano Lett.* **9** 3795
- [17] Meethong N, Huang H Y S, Carter W C and Chiang Y M 2007 *Electrochim. Solid St.* **10** A134
- [18] Wagemaker M, Mulder F M and van der Ven A 2009 *Adv. Mater.* **21** 2703
- [19] Wagemaker M, Singh D P, Borghols W J H, Lafont U, Haverkate L, Peterson V K and Mulder F M 2011 *J. Am. Chem. Soc.* **133** 10222
- [20] van der Ven A and Wagemaker M 2009 *Electrochim. Commun.* **11** 881
- [21] Meethong N, Kao Y H, Tang M, Huang H Y, Carter W C and Chiang Y M 2008 *Chem. Mater.* **20** 6189
- [22] Dreyer W, Jamnik J, Guhlke C, Huth R, Moskon J and Gaberscek M 2010 *Nat. Mater.* **9** 448
- [23] Jamnik J and Maier J 2003 *Phys. Chem. Chem. Phys.* **5** 5215
- [24] Ponrouach A, Taberna P L, Simon P and Palacin M R 2012 *Electrochim. Acta* **61** 13
- [25] Yamamoto K, Iriyama Y, Asaka T, Hirayama T, Fujita H, Nonaka K, Miyahara K, Sugita Y and Ogumi Z 2012 *Electrochim. Commun.* **20** 113
- [26] Yamamoto K, Hirayama T and Tanji T 2013 *Microscopy* **62** S29
- [27] Barsoukov E and Macdonald J R 2005 *Impedance Spectroscopy: Theory, Experiment, and Applications* (Wiley)
- [28] Bard A J and Faulkner L R 2000 *Electrochemical Methods: Fundamentals and Applications* (Wiley)
- [29] Vetter J, Novak P, Wagner M R, Veit C, Moller K C, Besenhard J O, Winter M, Wohlfahrt-Mehrens M, Vogler C and Hammouche A J 2005 *Power Sources* **147** 269
- [30] Ohzuku T and Brodd R J J 2007 *Power Sources* **174** 449
- [31] Jamnik J and Gaberscek M 2009 *Mrs Bull.* **34** 942
- [32] Kilic M S, Bazant M Z and Ajdari A 2007 *Phys. Rev. E* **75** 021502
- [33] Kilic M S, Bazant M Z and Ajdari A 2007 *Phys. Rev. E* **75** 021503
- [34] Bazant M Z, Thornton K and Ajdari A 2004 *Phys. Rev. E* **70** 021506
- [35] Zhao H 2011 *Phys. Rev. E* **84** 051504
- [36] Chu K T and Bazant M Z 2009 *Siam J. Appl. Math.* **65** 1485
- [37] Fuller T F, Doyle M and Newman J 1994 *J. Electrochim. Soc.* **141** 1
- [38] Latz A, Zausch J, and Iliev O 2011 *Lect. Notes Comput. Sci.* **6046** 329
- [39] Latz A, and Zausch J J 2011 *Power Sources* **196** 3296
- [40] Ceder G 2010 *Mrs Bull.* **35** 693
- [41] Hautier G, Fischer C C, Jain A, Mueller T and Ceder G 2010 *Chem. Mater.* **22** 3762
- [42] Fujimura K, Seko A, Koyama Y, Kuwabara A, Kishida I, Shitara K, Fisher C A J, Moriwake H and Tanaka I 2013 *Adv. Energy Mater.* **3** 980
- [43] Goodenough J B 2014 *Energy Environ. Sci.* **7** 14
- [44] Goodenough J B and Kim Y 2010 *Chem. Mater.* **22** 587
- [45] Goodenough J B and Kim Y J 2011 *Power Sources* **196** 6688
- [46] Goodenough J B 2012 *J. Solid State Electron.* **16** 2019
- [47] Goodenough J B 2013 *Accounts Chem. Res.* **46** 1053
- [48] Whittingham M S 2014 *Chem. Rev.* **114** 11414
- [49] Masquelier C and Croguennec L 2013 *Chem. Rev.* **113** 6552
- [50] Julien C M and Mauger A 2013 *Ionics* **19** 951

- [51] Tarascon J M, and Armand M 2001 *Nature* **414** 359
- [52] Kim T H, Park J S, Chang S K, Choi S, Ryu J H and Song H K 2012 *Adv. Energy Mater.* **2** 860
- [53] Hautier G, Jain A, Mueller T, Moore C, Ong S P and Ceder G 2013 *Chem. Mater.* **25** 2064
- [54] Hautier G, Jain A, Ong S P, Kang B, Moore C, Doe R and Ceder G 2011 *Chem. Mater.* **23** 3495
- [55] Aydinol M K, Kohan A F, Ceder G, Cho K and Joannopoulos J 1997 *Phys. Rev. B* **56** 1354
- [56] Ceder G, Chiang Y M, Sadoway D, Aydinol M, Jang Y I and Huang B 1998 *Nature* **392** 694
- [57] Ceder G 1998 *Science* **280** 1099
- [58] Tarascon J M, Wang E, Shokoohi F K, McKinnon W R and Colson S J 1991 *Electrochem. Soc.* **138** 2859
- [59] Bittihn R, Herr R and Hoge D J 1993 *Power Sources* **43** 223
- [60] Li G H, Ikuta H, Uchida T and Wakihara M 1996 *J. Electrochem. Soc.* **143** 178
- [61] Sigala C, Guyomard D, Verbaere A, Piffard Y and Tournoux M 1995 *Solid State Ionics* **81** 167
- [62] Amine K, Tukamoto H, Yasuda H and Fujita Y 1997 *J. Power Sources* **68** 604
- [63] Kawai H, Nagata M, Kageyama H, Tukamoto H and West A R 1999 *Electrochim. Acta* **45** 315
- [64] Ein-Eli Y, Howard W F, Lu S H, Mukerjee S, McBreen J, Vaughney J T and Thackeray M M 1998 *J. Electrochem. Soc.* **145** 1238
- [65] Zhong Q M, Bonakdarpour A, Zhang M J, Gao Y and Dahn J R 1997 *J. Electrochem. Soc.* **144** 205
- [66] Arroyo-de Dompablo M E, Armand M, Tarascon J M and Amador U 2006 *Electrochem. Commun.* **8** 1292
- [67] Padhi A K, Manivannan V and Goodenough J B 1998 *J. Electrochem. Soc.* **145** 1518
- [68] Yamada A 2014 *Mrs Bull.* **39** 423
- [69] Barpanda P, Nishimura S and Yamada A 2012 *Adv. Energy Mater.* **2** 841
- [70] Wang L, Li H, Huang X and Baudrin E 2011 *Solid State Ionics* **193** 32
- [71] Kim J H, Myung S T, Yoon C S, Kang S G and Sun Y K 2004 *Chem. Mater.* **16** 906
- [72] Arroyo-DeDompablo M E, Dominko R, Gallardo-Amores J M, Dupont L, Mali G, Ehrenberg H, Jamnik J and Moran E 2008 *Chem. Mater.* **20** 5574
- [73] Whittingham M S 1976 *Science* **192** 1126
- [74] Choi N S, Chen Z, Freunberger S A, Ji X, Sun Y K, Amine K, Yushin G, Nazar L F, Cho J and Bruce P G 2012 *Angew. Chem. Int. Edit.* **51** 9994
- [75] Manthiram A 2003 *Materials Aspects: An Overview* (in Lithium Batteries, Nazri G A and Pistoia G eds.) (New York: Springer)
- [76] Augustyn V and Manthiram A 2015 *Chem. Plus Chem.* **80** 422
- [77] Noh H J, Youn S, Yoon C S and Sun Y K 2013 *J. Power Sources* **233** 121
- [78] Poizot P, Laruelle S, Gruegeon S, Dupont L and Tarascon J M 2000 *Nature* **407** 496
- [79] Débart A, Dupont L, Poizot P, Leriche J B and Tarascon J M 2001 *J. Electrochem. Soc.* **148** A1266
- [80] Poizot P, Laruelle S, Gruegeon S and Tarascon J M 2002 *J. Electrochem. Soc.* **149** A1212
- [81] Larcher D, Sudant G, Leriche J B, Chabre Y and Tarascon J M 2002 *J. Electrochem. Soc.* **149** A234
- [82] Li H, Richter G and Maier J 2003 *Adv. Mater.* **15** 736
- [83] Badway F, Pereira N, Cosandey F and Amatucci G G 2003 *J. Electrochem. Soc.* **150** A1209
- [84] Balaya P, Li H, Kienle L and Maier J 2003 *Adv. Funct. Mater.* **13** 621
- [85] Silva D C C, Crozier O, Ouvrard G, Greidanus J, Safa-Sefat A and Nazar L F 2003 *Electrochem. Solid States* **6** A162
- [86] Fu Z W, Wang Y, Yue X L, Zhao S L and Qin Q Z 2004 *J. Phys. Chem. B* **108** 2236
- [87] Fu Z W, Li C L, Liu W Y, Ma J, Wang Y and Qin Q Z 2005 *J. Electrochem. Soc.* **152** E50
- [88] Bréger J, Meng Y S, Hinuma Y, Kumar S, Kang K, Shao-Horn Y, Ceder G and Grey C P 2006 *Chem. Mater.* **18** 4768
- [89] Delacourt C, Poizot P, Tarascon J M and Masquelier C 2005 *Nat. Mater.* **4** 254
- [90] Dodd J L, Yazami R and Fultz B 2006 *Electrochem. Solid States* **9** A151
- [91] Zhou F, Maxisch T and Ceder G 2006 *Phys. Rev. Lett.* **97** 155704
- [92] Taberna L, Mitra S, Poizot P, Simon P and Tarascon J M 2006 *Nat. Mater.* **5** 567
- [93] Doe R E, Persson K A, Meng Y S and Ceder G 2008 *Chem. Mater.* **20** 5274
- [94] Sholl D S and Steckel J A 2009 *Accuracy and Methods beyond "Standard" Calculations Density Functional Theory* (John Wiley & Sons, Inc)
- [95] Ceder G, Aydinol M K and Kohan A F 1997 *Comput. Mater. Sci.* **8** 161
- [96] Morgan D, Ceder G, Saidi M Y, Barker J, Swoyer J, Huang H and Adamson G J 2003 *Power Sources* **119** 755
- [97] Morgan D, Ceder G, Saidi M Y, Barker J, Swoyer J, Huang H and Adamson G 2002 *Chem. Mater.* **14** 4684
- [98] Zhou F, Cococcioni M, Marianetti C A, Morgan D and Ceder G 2004 *Phys. Rev. B* **70** 235121
- [99] Chevrier V L, Ong S P, Armiento R, Chan M K Y and Ceder G 2010 *Phys. Rev. B* **82** 075122